Aircraft Fault-Tolerant Trajectory Control Using Incremental Nonlinear Dynamic Inversion

Article *in* Control Engineering Practice · September 2016

DOI: 10.1016/j.conengprac.2016.09.010

CITATIONS
99

READS
1,017

4 authors:

Peng Lu
The University of Hong Kong
68 PUBLICATIONS **1,235** CITATIONS
SEE PROFILE

Erik-Jan Van Kampen
Delft University of Technology
217 PUBLICATIONS **2,809** CITATIONS
SEE PROFILE

Coen De Visser
Delft University of Technology
180 PUBLICATIONS **2,070** CITATIONS
SEE PROFILE

Q.P. Chu
265 PUBLICATIONS **5,584** CITATIONS
SEE PROFILE

Aircraft Fault-Tolerant Trajectory Control Using Incremental Nonlinear Dynamic Inversion

Peng Lu[a,*], Erik-Jan van Kampen[a], Cornelis de Visser[a], Qiping Chu[a]

[a] *Delft University of Technology, Kluyverweg 1, 2629HS Delft, The Netherlands*

Abstract

This paper deals with aircraft trajectory control in the presence of model uncertainties and actuator faults. Existing approaches, such as adaptive backstepping and nonlinear dynamic inversion with online model identification, can be applied. However, since there are a number of unknown aerodynamic derivatives, the tuning of parameter update law gains is time-consuming. Methods with online model identification require excitation and the selection of a threshold. Furthermore, to deal with highly nonlinear aircraft dynamics, the aerodynamic model structure needs to be designed. In this paper, a novel aircraft trajectory controller, which uses the Incremental Nonlinear Dynamic Inversion, is proposed to achieve fault-tolerant trajectory control. The detailed control law design of four loops is presented. The idea is to design the loops with uncertainties using the incremental approach. The tuning of the approach is straightforward and there is no requirement for excitation and selection of a threshold. The performance of the proposed controller is compared with existing approaches using three scenarios. The results show that the proposed trajectory controller can follow the reference even when there are model uncertainties and actuator faults.

Keywords: Trajectory control, Fault-Tolerant Control, nonlinear flight control, Incremental Nonlinear Dynamic Inversion, model identification

*Corresponding author.

Email addresses: P.Lu-1@tudelft.nl (Peng Lu), E.vanKampen@tudelft.nl (Erik-Jan van Kampen), c.c.devisser@tudelft.nl (Cornelis de Visser), q.p.chu@tudelft.nl (Qiping Chu)

Nomenclature

A_x, A_y, A_z	=	specific forces along the body axis, m/s^2
u_a, v_a, w_a	=	airspeed velocity components along the body axis, m/s
x, y, z	=	position coordinates in the earth fixed reference frame, m
X, Y, Z	=	aerodynamic forces including thrust forces along the body axis, N
L, M, N	=	aerodynamic moments including thrust moments along the body axis, N
$\bar{q}$	=	dynamic pressure, Pa
S	=	wing surface area, m/s^2
$\bar{c}$, b	=	mean aerodynamic chord and wing span, m
V	=	total velocity, m/s
χ	=	kinematic azimuth angle, rad
γ	=	flight path angle, rad
μ	=	kinematic roll angle, rad
$\mathbf{u}$, $\Delta\mathbf{u}$	=	input and incremental input
α, β	=	angle of attack, sideslip angle, rad
ϕ, θ, ψ	=	roll, pitch and yaw angles along the body axis with respect to the Earth frame, rad
p, q, r	=	roll, pitch and yaw rate along the body axis, rad/s
PLA	=	power level angle, rad
$\Delta\delta_a$, $\Delta\delta_e$, $\Delta\delta_r$	=	incremental deflections of the aileron, elevator and rudder, rad
δ_a, δ_e, δ_r	=	deflections of the ailerons, elevators and rudders, rad
δ_{ar}, δ_e, δ_{rl}	=	deflections of the right aileron, elevator and lower rudder, rad
δ_{al}, δ_e, δ_{ru}	=	deflections of the left aileron and upper rudder, rad
Superscripts		
des		desired reference value generated by the controller
ref		reference value given to the controller
exp		expected value

1. Introduction

Civil aircraft are usually required to follow trajectories in three-dimensional space, such as those imposed by air traffic control [1]. In the design phase of civil aircraft, safety is of critical concern. Many techniques [2, 3, 4, 5, 6, 7, 8, 9, 10, 11] have been proposed to improve the safety level and reduce critical risks. Conventionally, since the aircraft model is nonlinear, flight control systems are designed based on a number of linearized models around certain operating points [3]. Next, a gain scheduling method has to be used to blend the gains in different operating points into one controller.

Using nonlinear control approaches, design of different operating points can be avoided. Linearization-based methods, such as Nonlinear Dynamic Inversion (NDI) and Backstepping (BS), are nonlinear control methods which can handle nonlinearities in the model. This paper also makes use of nonlinear control methods to design a trajectory controller. Aircraft trajectory control has been considered by several researchers [1, 12, 13, 14, 15, 16, 17]. To design the trajectory controller, the uncertainties of aerodynamic derivatives have to be considered since they can degrade the performance of the nonlinear control approaches. [12] uses a sliding mode adaptive controller to reduce the influence of uncertainties. In [13], a control Lyapunov function approach is applied. In [14], a Command Filtered Backstepping approach which uses adaptive function approximation is applied to design the trajectory controller. [17] deals with model uncertainties using the NDI method. The influence of model uncertainties is decreased by making use of a concurrent learning approach [17]. [15] applies Adaptive Backstepping (ABS) [18, 19] with parameter update laws. However, the computational load of the ABS is intensive and the tuning of the parameter update law gains is time-consuming [20]. In [16, 21], NDI is used to deal with the nonlinearities and the model uncertainties influence is reduced by identifying the unknown parameters online. The method is validated on the SIMONA (SImulation, MOtion and NAvigation) research simulator [16]. However, this method is based on parameter identification and it requires excitation [16] which could limit its performance when there is no excitation. Furthermore, to deal with highly nonlinear aircraft dynamics, an aerodynamic model structure needs to be designed [22].

The present paper proposes a novel nonlinear controller for aircraft trajectory control. The NDI-based approach is used to deal with nonlinearities in the model. The solution to cope with uncertain aerodynamic derivatives is to make use of Incremental Nonlinear Dynamic Inversion (INDI) [23, 24, 25]. A control structure with four loops are designed: position control, flight path control, attitude and angular rate control. Through analysis, it is found that there are only model uncertainties in the flight path and angular rate control loops. Therefore, these two control loops are designed based on the INDI control law while the remaining two control loops are designed based on the NDI control law. An additional benefit of using the proposed approach is that there is no need to design the aerodynamic model structure. The overall control architecture of the trajectory controller and the detailed design are presented in the paper.

The performance of our approach is compared to the approach proposed in [16]. The model-based approach in [16] requires sufficient excitation, which may be difficult to obtain during failure situations. The performance comparison is perform using three scenarios: no fault, model uncertainties, and actuator faults. All three scenarios demonstrate the performance of the proposed trajectory controller.

The faults considered in this paper only include actuator faults. For Fault-Tolerant Control (FTC) in the presence of sensor faults, the reader is referred to [26, 27, 28, 29, 30].

The structure of this paper is as follows: Section 2 presents the aircraft model which is used for designing the trajectory controller. In Section 3, the four control loops and the distribution of model uncertainties are

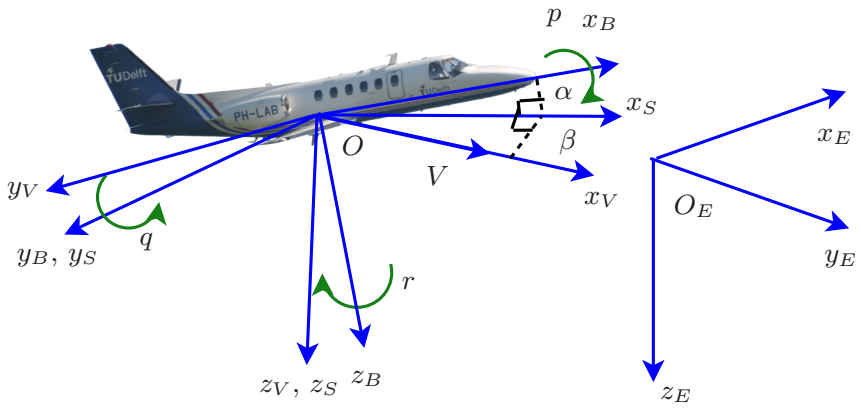

Figure 1: Aircraft reference frames

introduced. The detailed control law design is given in Section 4. The position control and attitude control loops are designed based on the NDI control approach while the flight path control and angular rate control loops are designed based on the INDI control approach. In Section 5, the aircraft model and fault scenario are presented. The baseline controller, Nonlinear Dynamic Inversion with model identification (NDI-MI), is also presented. In Section 6, the performance of the proposed trajectory controller is compared to existing method which is the NDI-MI. Their performances are compared under three scenarios. Finally, the conclusions are given in Section 7.

2. Aircraft equations of motion

In this section, the aircraft model used for designing the control law is described. It is assumed that the Earth is flat and non-rotating. Under this condition, the Earth-center Earth-fixed reference frame is equal to the Earth-fixed inertial reference frame. The body reference frame ($Ox_By_Bz_B$), Earth-center Earth-fixed reference frame ($O_Ex_Ey_Ez_E$), stability reference frame ($Ox_Sy_Sz_S$) and velocity reference frame ($Ox_Vy_Vz_V$) are shown in Fig. 1.

Define the inertial position vector of the aircraft as follows:

$$\mathbf{x}_0 = [x, y, z]^T \tag{1}$$

where x, y and z denote the position of the aircraft in the North, East and down directions. The derivatives of the position vector are:

$$\dot{\mathbf{x}}_0 = \begin{bmatrix} V\cos\chi\cos\gamma \\ V\sin\chi\cos\gamma \\ -V\sin\gamma \end{bmatrix} \tag{2}$$

Define:

$$\mathbf{x}_1 = [V, \chi, \gamma]^T \tag{3}$$

where V is the total velocity of the aircraft, χ is the kinematic azimuth angle and γ is the flight path angle. The dynamics of $\mathbf{x}_1$ are [31]:

$$\dot{\mathbf{x}}_1 = \begin{bmatrix} 1 & 0 & 0 \\ 0 & \frac{1}{V\cos\gamma} & 0 \\ 0 & 0 & -1/V \end{bmatrix} \mathbf{T_{VB}} \frac{\mathbf{F}_B}{m} \tag{4}$$

$$= \begin{bmatrix} \frac{1}{m} & 0 & 0 \\ 0 & \frac{1}{mV\cos\gamma} & 0 \\ 0 & 0 & \frac{-1}{mV} \end{bmatrix} \left(\mathbf{T_{VB}} \begin{bmatrix} X \\ Y \\ Z \end{bmatrix} + \mathbf{T_{VE}} \begin{bmatrix} 0 \\ 0 \\ mg \end{bmatrix} \right) \tag{5}$$

where $\mathbf{F}_B$ represent the total forces (including aerodynamic, propulsion and gravitational forces) acting on the aircraft expressed in the body reference frame. X, Y and Z denote the sum of aerodynamic and propulsion forces expressed in the body axes. $\mathbf{T_{VB}}$ is the transformation matrix from the body frame to the velocity frame and $\mathbf{T_{VE}}$ is the transformation matrix from the Earth frame to the velocity frame. These matrices are given as:

$$\mathbf{T_{VB}} = \begin{bmatrix} \cos\alpha\cos\beta & \sin\beta & \sin\alpha\cos\beta \\ -\cos\alpha\sin\beta\cos\mu + \sin\alpha\sin\mu & \cos\beta\cos\mu & -\sin\alpha\sin\beta\cos\mu - \cos\alpha\sin\mu \\ -\cos\alpha\sin\beta\sin\mu - \sin\alpha\cos\mu & \cos\beta\sin\mu & -\sin\alpha\sin\beta\sin\mu + \cos\alpha\cos\mu \end{bmatrix} \tag{6}$$

$$\mathbf{T_{VE}} = \begin{bmatrix} \cos\chi\cos\gamma & \sin\chi\cos\gamma & -\sin\gamma \\ -\sin\chi & \cos\chi & 0 \\ \cos\chi\sin\gamma & \sin\chi\sin\gamma & \cos\gamma \end{bmatrix} \tag{7}$$

The attitude angles are defined as:

$$\mathbf{x}_2 = [\mu, \alpha, \beta]^T \tag{8}$$

where μ is the kinematic bank angle. α and β are the aerodynamic angle of attack and angle of sideslip, respectively. Their kinematics are given as follows [31]:

$$\dot{\mathbf{x}}_2 = \begin{bmatrix} \cos\alpha\cos\beta & 0 & \sin\alpha \\ \sin\beta & 1 & 0 \\ \sin\alpha\cos\beta & 0 & -\cos\alpha \end{bmatrix}^{-1} \left(-\mathbf{T_{BV}} \begin{bmatrix} -\dot{\chi}\sin\gamma \\ \dot{\gamma} \\ \dot{\chi}\cos\gamma \end{bmatrix} + \begin{bmatrix} p \\ q \\ r \end{bmatrix} \right) \tag{9}$$

It should be noted that μ is not directly measured onboard. It is integrated from Eq. (9).

Further define

$$\mathbf{x}_3 = \boldsymbol{\omega} = [p, q, r]^T \tag{10}$$

The dynamics of the angular rates of the aircraft are presented as follows [31]:

$$\dot{\boldsymbol{\omega}} = \mathbf{J}^{-1}(\mathbf{M} - \boldsymbol{\omega} \times \mathbf{J}\boldsymbol{\omega}) \tag{11}$$

where $\mathbf{J}$ is the inertia matrix defined as

$$\mathbf{J} = \begin{bmatrix} I_{xx} & -I_{xy} & -I_{xz} \\ -I_{xy} & I_{yy} & -I_{yz} \\ -I_{xz} & -I_{yz} & I_{zz} \end{bmatrix} \tag{12}$$

$\mathbf{M}$ are the total moments acting on the aircraft which can be split into two parts:

$$\mathbf{M} = \mathbf{M}_a + \mathbf{M}_u = \mathbf{M}_a + \mathbf{C}_{\mathbf{M_u}}\mathbf{u} \tag{13}$$

where $\mathbf{M}_u$ are the moments generated by the control surface deflections and $\mathbf{M}_a$ are all moments except for $\mathbf{M}_u$. $\mathbf{C}_{\mathbf{M_u}}$ are the coefficients related to $\mathbf{M}_u$, which are denoted as

$$\mathbf{C}_{\mathbf{M_u}} = \bar{q}S\mathbf{C}_1 \begin{bmatrix} C_{l_{\delta a}} & 0 & C_{l_{\delta r}} \\ 0 & C_{m_{\delta e}} & 0 \\ C_{n_{\delta a}} & 0 & C_{n_{\delta r}} \end{bmatrix}, \mathbf{C}_1 = \mathrm{diag}(b, \bar{c}, b) \tag{14}$$

where $\bar{q}$ is the dynamic pressure, S is the wing area, b the wing span and $\bar{c}$ is the mean aerodynamic chord. The control surface deflections are $\mathbf{u} = [\delta_a \quad \delta_e \quad \delta_r]^T$, which are also the input to the system.

Eq. (11) can be rewritten into the following affine-in-control form:

$$\dot{\mathbf{x}}_3 = \mathbf{f}_3 + \mathbf{G}_3\mathbf{u} \tag{15}$$

where $\mathbf{f}_3 = \mathbf{J}^{-1}(\mathbf{M}_a - \boldsymbol{\omega} \times \mathbf{J}\boldsymbol{\omega})$, $\mathbf{G}_3 = \mathbf{J}^{-1}\mathbf{C}_{\mathbf{M_u}}$.

3. Control loops and uncertainty sources

In this section, the control loops and the relationships among them are given. Then, the uncertainty sources are presented.

For the ease of explanation, define the following variables:

$$\mathbf{x}_0^{ref} = [x^{ref}, y^{ref}, z^{ref}]^T, \ \mathbf{x}_1^{des} = [V^{ref}, \chi^{des}, \gamma^{des}]^T \tag{16}$$

$$\mathbf{x}_2^{'des} = [PLA^{des}, \mu^{des}, \alpha^{des}]^T, \ \mathbf{x}_2^{des} = [\mu^{des}, \alpha^{des}, \beta^{ref}]^T \tag{17}$$

$$\mathbf{x}_3^{des} = [p^{des}, q^{des}, r^{des}]^T, \ \mathbf{u}^{des} = [\delta_a^{des}, \delta_e^{des}, \delta_r^{des}]^T \tag{18}$$

where superscript ref and des both denote the reference commands for corresponding variables. The difference between them is that ref denotes the reference commands which are given for the controller to follow and des denotes the desired reference commands generated by the controller.

The control law design is based on the following four loops:

1. Position control loop

   The objective of this control loop is to follow the trajectory reference $\mathbf{x}_0^{ref}$. The desired references χ^{des} and γ^{des} are generated in this loop.

2. Flight path control loop

   The objective of this loop is to steer $\mathbf{x}_1$ to the given references $\mathbf{x}_1^{des}$. It generates the desired commands μ^{des} and α^{des} for the attitude control loop. In addition, to follow the velocity reference V^{des}, it generates the desired power level angle PLA^{des} for the engine.

3. Attitude control loop

   The objective of this control loop is to follow $\mathbf{x}_2^{des}$ given by the flight path control loop. To control the attitude, it provides the desired command $\mathbf{x}_3^{des}$ for the angular rate control loop.

4. Angular rate control loop

   This loop follows $\mathbf{x}_3^{des}$ given by the attitude control loop. To achieve the objective, it provides the desired command $\mathbf{u}^{des}$ to the actuators such that the control goal can be achieved.

To compute the control law, the aerodynamic forces and moments need to be calculated. The aerodynamic forces acting on the aircraft expressed in the body axis, denoted by $\mathbf{F}_B$, change the flight path, as described in Eq. (4). The aerodynamic moments generated by the control surfaces (ailerons, elevators and rudders), modify the angular rates, as described in Eq. (11). The attitude control loop contains no model uncertainties, as seen in Eq. (9).

The aerodynamic forces can be expressed by Taylor series [32]. For instance, X can be expanded as follows (higher-order terms are neglected for simplicity of explanation):

$$X = \bar{q}SC_X = \bar{q}S(C_{X_0} + C_{X_\alpha}\alpha + C_{X_q}\frac{q\bar{c}}{V} + C_{X_{\delta_e}}\delta_e + C_{X_{PLA}}PLA) \tag{19}$$

where δ_e is the deflection angle of the elevator and PLA represents power level angle. C_{X_α} and C_{X_q} are stability derivatives. $C_{X_{\delta_e}}$ and $C_{X_{PLA}}$ are control derivatives. These derivatives can vary according to various flight conditions and are therefore not constant. To obtain these parameters, computer fluid dynamics or wind tunnel tests are usually performed. However, accurate parameters in various flight situations are difficult to obtain which leads to model uncertainties. Likewise, the aerodynamic moments can also be expressed in Taylor series. M can be expressed as

$$M = \bar{q}SC_M = \bar{q}S(C_{M_0} + C_{M_\alpha}\alpha + C_{M_q}\frac{q\bar{c}}{V} + C_{M_{\delta_e}}\delta_e + C_{M_{PLA}}PLA) \tag{20}$$

where C_{M_α} and C_{M_q} are stability derivatives. $C_{M_{\delta_e}}$ and $C_{M_{PLA}}$ are the control derivatives. Inaccurate C_{M_α}, C_{M_q}, $C_{M_{\delta_e}}$ and $C_{M_{PLA}}$ bring model uncertainties in the control law design and can result in performance degradation.

The uncertainties in these parameters must be taken into account when designing the control laws. Researchers have proposed many adaptive controllers [18, 20, 33, 34] which consider model uncertainties.

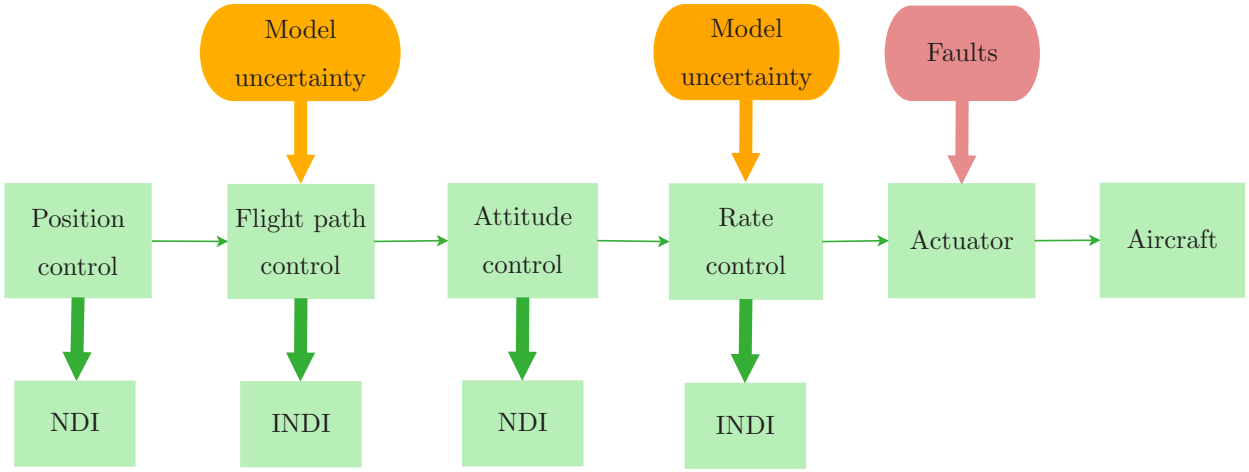

Figure 2: Distributions of the model uncertainties and controllers

For instance, ABS [18, 33] approaches are proposed which estimate the unknown aerodynamic forces and moments by updating the parameter estimate through a specific update law. However, since there are many parameters to be estimated, the tuning of the update law gains is time-consuming [20] and the adaptive controller is computationally intensive [20]. In this paper, the idea is to design the control loop which has model uncertainties using an incremental control approach. Since model uncertainties only exist in the flight path control loop and the angular rate control loop, the incremental approach design is only applied to these two control loops. This can be seen in Fig. 2. The other two loops, position control loop and attitude control loop, are designed based on the standard NDI approach [35].

4. Trajectory control law design

In this section, the design of the control law for the four loops is presented. Finally, the overall control architecture is presented.

4.1. Position control loop

The position control contains no model uncertainties and is designed based on the NDI control law. It is assumed that the reference trajectory is generated through

$$\begin{bmatrix} \dot{x}^{ref} \\ \dot{y}^{ref} \\ \dot{z}^{ref} \end{bmatrix} = \begin{bmatrix} V^{ref} \cos\chi^{ref} \cos\gamma^{ref} \\ V^{ref} \sin\chi^{ref} \cos\gamma^{ref} \\ -V^{ref} \sin\gamma^{ref} \end{bmatrix} \tag{21}$$

In this paper, we also try to follow the reference V^{ref}. Through the last two equations of Eq. (2), the desired reference commands for χ and γ can be calculated based on the standard NDI approach [35] as follows (See

Appendix C in [36] for the design principle of NDI):

$$\begin{bmatrix} \chi^{des} \\ \gamma^{des} \end{bmatrix} = \begin{bmatrix} \arcsin(\nu_y/(V^{ref}\cos\gamma)) \\ -\arcsin(\nu_z/(V^{ref})) \end{bmatrix} \tag{22}$$

where ν_y and ν_z are virtual controls which can be designed using classical linear control such as a Proportional-Integral-Derivative control as follows:

$$\nu_y(t) = K_P^p e_y(t) + K_I^p \int_0^t e_y(\tau)d\tau + K_D^p \frac{de_y(t)}{dt} \tag{23}$$

$$\nu_z(t) = K_P^p e_z(t) + K_I^p \int_0^t e_z(\tau)d\tau + K_D^p \frac{de_z(t)}{dt} \tag{24}$$

where

$$e_y(t) = y^{ref}(t) - y(t) \tag{25}$$

$$e_z(t) = z^{ref}(t) - z(t). \tag{26}$$

and K_P^p, K_I^p and K_D^p are the gains for the position control loop.

4.2. Flight path control loop

The flight path control loop requires the calculation of the aerodynamic forces, which contains model uncertainties. Therefore, it needs to be designed based on the incremental approach.

4.2.1. Design of μ^{des}

In the flight path control loop, the objective is to steer V, χ and γ to their references denoted as V^{ref}, χ^{des} and γ^{des}. The virtual control variables are μ, α and PLA. However, μ, α and PLA do not appear affine in Eq. (5). Therefore, the equation needs to be rewritten to be in the affine-in-control form.

Express the forces X and Z as follows:

$$X = \bar{q}SC_X = \bar{q}S(C_{X_0} + C_{X_\alpha}\alpha + C_{X_q}\frac{q\bar{c}}{V} + C_{X_{\delta_e}}\delta_e + C_{X_{PLA}}PLA) \tag{27}$$

$$Z = \bar{q}SC_Z = \bar{q}S(C_{Z_0} + C_{Z_\alpha}\alpha + C_{Z_q}\frac{q\bar{c}}{V} + C_{Z_{\delta_e}}\delta_e + C_{Z_{PLA}}PLA) \tag{28}$$

Since the virtual control variables are μ, α and PLA, Eqs. (27) and (28) can be rewritten into the following:

$$X = \bar{q}SC_X = \bar{q}S(\bar{C}_{X_0} + C_{X_\alpha}\alpha + C_{X_{PLA}}PLA) \tag{29}$$

$$Z = \bar{q}SC_Z = \bar{q}S(\bar{C}_{Z_0} + C_{Z_\alpha}\alpha + C_{Z_{PLA}}PLA) \tag{30}$$

where

$$\bar{C}_{X_0} = C_X - C_{X_\alpha}\alpha - C_{X_{PLA}}PLA \tag{31}$$

$$\bar{C}_{Z_0} = C_Z - C_{Z_\alpha}\alpha - C_{Z_{PLA}}PLA \tag{32}$$

Express Y as $Y = mA_y$ and substitute it with Eqs. (29) and (30) into Eq. (5), it follows

$$\dot{\mathbf{x}}_1 = \begin{bmatrix} \frac{1}{m} & 0 & 0 \\ 0 & \frac{1}{mV\cos\gamma} & 0 \\ 0 & 0 & \frac{-1}{mV} \end{bmatrix} \left(\mathbf{T_{VB}} \begin{bmatrix} \bar{q}S(\bar{C}_{X_0} + C_{X_{PLA}} PLA + C_{X_\alpha}\alpha \\ mA_y \\ \bar{q}S(\bar{C}_{Z_0} + C_{Z_{PLA}} PLA + C_{Z_\alpha}\alpha \end{bmatrix} + \mathbf{T_{VE}} \begin{bmatrix} 0 \\ 0 \\ mg \end{bmatrix} \right) \tag{33}$$

In the attitude control loop, β should be kept at zero. Therefore, it is reasonable to assume that β is close to zero. Under this condition, Eq. (33) can be further simplified into

$$\dot{\mathbf{x}}_1 = \begin{bmatrix} \frac{1}{m} & 0 & 0 \\ 0 & \frac{1}{mV\cos\gamma} & 0 \\ 0 & 0 & -\frac{1}{mV} \end{bmatrix} \left(\begin{bmatrix} \cos\alpha & 0 & \sin\alpha \\ \sin\alpha\sin\mu & \cos\mu & -\cos\alpha\sin\mu \\ -\sin\alpha\cos\mu & \sin\mu & \cos\alpha\cos\mu \end{bmatrix} \begin{bmatrix} \bar{q}S(\bar{C}_{X_0} + C_{X_{PLA}} PLA + C_{X_\alpha}\alpha) \\ mA_y \\ \bar{q}S(\bar{C}_{Z_0} + C_{Z_{PLA}} PLA + C_{Z_\alpha}\alpha) \end{bmatrix} + \begin{bmatrix} -mg\sin\gamma \\ 0 \\ mg\cos\gamma \end{bmatrix} \right) \tag{34}$$

First, let us derive μ^{des}. Due to $X = mA_x$ and $Z = mA_z$, the last two equations of Eq. (34) can be written as:

$$\dot{\chi} = \frac{1}{V\cos\gamma}(A_x\sin\alpha\sin\mu + A_y\cos\mu - A_z\cos\alpha\sin\mu) \tag{35}$$

$$\dot{\gamma} = \frac{1}{V}(A_x\sin\alpha\cos\mu - A_y\sin\mu - A_z\cos\alpha\cos\mu - g\cos\gamma) \tag{36}$$

Rewrite Eqs. (35) and (36) into the following form:

$$(A_x\sin\alpha - A_z\cos\alpha)\sin\mu = V\cos\gamma\dot{\chi} - A_y\cos\mu \tag{37}$$

$$(A_x\sin\alpha - A_z\cos\alpha)\cos\mu = V\dot{\gamma} + A_y\sin\mu + g\cos\gamma \tag{38}$$

The desired command μ^{des} can be designed as follows:

$$\mu^{des} = \arctan\frac{\nu_\chi V\cos\gamma - A_y\cos\mu}{\nu_\gamma V + A_y\sin\mu + g\cos\gamma} \tag{39}$$

where ν_χ and ν_γ are the virtual controls which are designed in the same way as ν_y and ν_z which are given in Eqs. (23) and (24). If further assume that A_y is small, the control law can be further simplified as follows:

$$\mu^{des} = \arctan\frac{\nu_\chi V\cos\gamma}{\nu_\gamma V + g\cos\gamma} \tag{40}$$

4.2.2. Design of PLA^{des} and α^{des}

Next, the design of the desired commands PLA^{des} and α^{des} is presented. The design of PLA^{des} and α^{des} is different from that of μ^{des}. This is because there are model uncertainties in the first and third equations of Eq. (34). Therefore, they should be designed using the incremental approach.

In order to design the incremental control law, the system dynamics need to be written into the incremental control form. First, write the first and third equations of Eq. (34) into:

$$\dot{\bar{\mathbf{x}}}_1 = \bar{\mathbf{f}}_1(\mathbf{x}_1, \mathbf{x}_2) + \bar{\mathbf{g}}_1 \bar{\mathbf{x}}_2 \tag{41}$$

where

$$\bar{\mathbf{x}}_1 = [V, \gamma]^T, \bar{\mathbf{x}}_2 = [PLA, \alpha]^T \tag{42}$$

$$\bar{\mathbf{f}}_1 = \begin{bmatrix} -g\sin\gamma + \frac{\bar{q}S}{m}(\bar{C}_{X_0}\cos\alpha + \bar{C}_{Z_0}\sin\alpha) \\ -\frac{A_y \sin\mu}{V} - \frac{g\cos\gamma}{V} - \frac{\bar{q}S}{mV}(-\bar{C}_{X_0}\sin\alpha\cos\mu + \bar{C}_{Z_0}\cos\alpha\cos\mu) \end{bmatrix} \tag{43}$$

$$\bar{\mathbf{g}}_1 = \frac{\bar{q}S}{mV}\begin{bmatrix} V(C_{X_{PLA}}\cos\alpha + C_{Z_{PLA}}\sin\alpha) & V(C_{X_\alpha}\cos\alpha + C_{Z_\alpha}\sin\alpha) \\ C_{X_{PLA}}\sin\alpha\cos\mu - C_{Z_{PLA}}\cos\alpha\cos\mu & C_{X_\alpha}\sin\alpha\cos\mu - C_{Z_\alpha}\cos\alpha\cos\mu \end{bmatrix} \tag{44}$$

According to [23, 24, 37], Eq. (41) can be written into the following incremental control form:

$$\dot{\bar{\mathbf{x}}}_1 = \dot{\bar{\mathbf{x}}}_{1,0} + \bar{\mathbf{g}}_1 \Delta\bar{\mathbf{x}}_2 \tag{45}$$

where

$$\dot{\bar{\mathbf{x}}}_{1,0} = \bar{\mathbf{f}}_1(\bar{\mathbf{x}}_{1,0}, \bar{\mathbf{x}}_{2,0}) + \bar{\mathbf{g}}_1 \bar{\mathbf{x}}_{2,0} \tag{46}$$

where $\bar{\mathbf{x}}_{1,0}$ and $\bar{\mathbf{x}}_{2,0}$ denote $\bar{\mathbf{x}}_1$ and $\bar{\mathbf{x}}_2$ at the last time step. $\dot{\bar{\mathbf{x}}}_{1,0}$ denotes the derivative of $\bar{\mathbf{x}}_1$ at the last time step.

Then the desired virtual incremental input $\Delta\bar{\mathbf{x}}_2$ can be designed by (See Appendix C in [36] for the design principle of INDI)

$$\Delta\bar{\mathbf{x}}_2 = \bar{\mathbf{g}}_1^{-1}(\nu_{\bar{\mathbf{x}}_1} - \dot{\bar{\mathbf{x}}}_{1,0}) \tag{47}$$

where $\nu_{\bar{\mathbf{x}}_1} = [\nu_V, \nu_\gamma]^T$ is designed based on the errors between V, γ and V^{ref}, γ^{des}.

The final desired command for $\bar{\mathbf{x}}_2$ can be given by

$$\bar{\mathbf{x}}_2^{des} = \bar{\mathbf{x}}_{2,0} + \Delta\bar{\mathbf{x}}_2 \tag{48}$$

There are two engines, of which the desired references PLA_1^{des} and PLA_2^{des} are both equal to PLA^{des}.

4.2.3. Calculation of the derivatives $\dot{\bar{x}}_{1,0}$

$\dot{\bar{\mathbf{x}}}_{1,0}$ can be calculated using different approaches. It can be calculated using the sliding mode differentiator [38]. Alternatively, it can also be obtained using a second-order low-pass filter. According to [23], $\dot{\bar{\mathbf{x}}}_{1,0}$ can be computed by passing $\bar{\mathbf{x}}_{1,0}$ through the following washout filter:

$$\frac{s\omega_n^2}{s^2 + 2\zeta_n\omega_n s + \omega_n^2} \tag{49}$$

with $\zeta_n = 0.8$, $\omega_n = 25$ rad/s. These are selected by trial and error to reduce the influence of noise [23].

The overall block diagram of the flight path control loop is shown in Fig. 3. It can be noted in the figure that to calculate $\bar{x}_{2,0}$, a second-order filter is used to counteract the influence of phase delay [39].

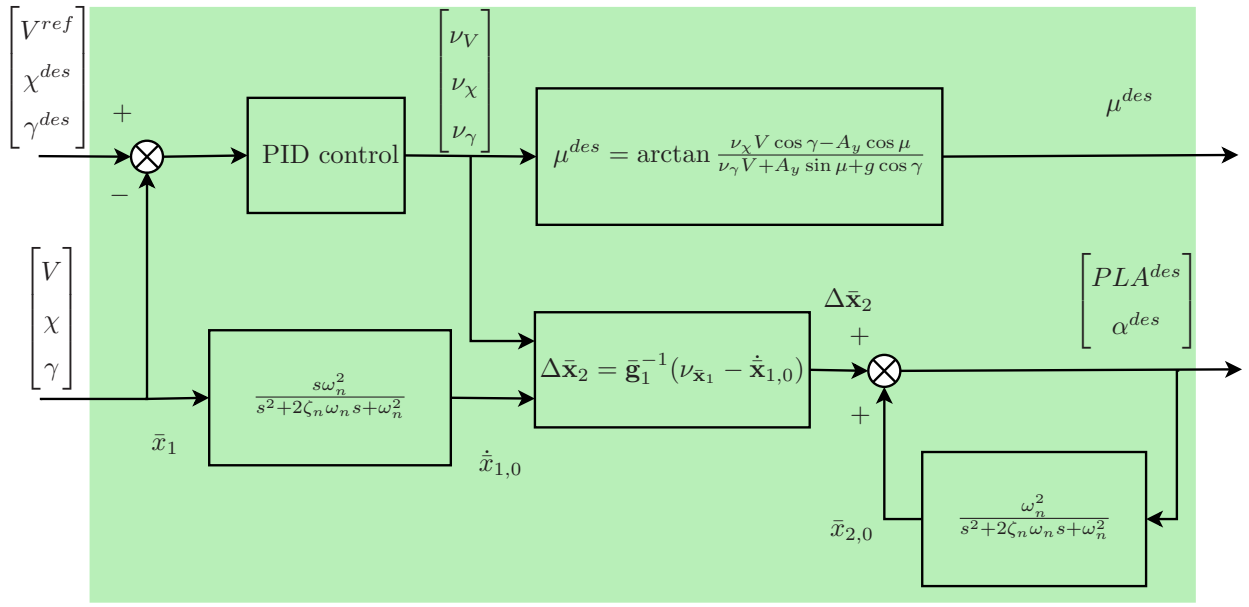

Figure 3: Block diagram of the flight path control loop

4.3. Attitude control loop

In this control loop, the objective is to follow μ^{des}, α^{des} and β^{ref}. μ^{des}, α^{des} have already been given in the flight path control loop. β^{ref} is set to zero to enable coordinated turns. The virtual control variables are the angular rates $\boldsymbol{\omega}$. In this control loop, there is no model uncertainty. Therefore, there is no need to design an incremental control law.

The desired virtual control law, based on the standard NDI approach [35], is given as follows (See Appendix C in [36] for the design principle of NDI):

$$\begin{bmatrix} p^{des} \\ q^{des} \\ r^{des} \end{bmatrix} = \begin{bmatrix} \cos\alpha\cos\beta & 0 & \sin\alpha \\ \sin\beta & 1 & 0 \\ \sin\alpha\cos\beta & 0 & -\cos\alpha \end{bmatrix} \begin{bmatrix} \nu_\mu \\ \nu_\alpha \\ \nu_\beta \end{bmatrix} + \mathbf{T_{BV}} \begin{bmatrix} -\dot{\chi}\sin\gamma \\ \dot{\gamma} \\ \dot{\chi}\cos\gamma \end{bmatrix} \tag{50}$$

where $\mathbf{T_{BV}} = \mathbf{T_{VB}^T}$. ν_μ, ν_α and ν_β are virtual controls designed based on the errors between μ^{des}, α^{des}, β^{ref} and μ, α, β. It is seen from Eq. (50) that in order to calculate the virtual control law, $\dot{\chi}$ and $\dot{\gamma}$ are required. This can be calculated using Eqs. (35) and (36). In these equations, A_x, A_y and A_z are directly measured by the accelerometers of the aircraft.

4.4. Angular rate control loop

In this control loop, the control objective is to follow the angular rate references generated by the attitude control loop denoted as p^{des}, q^{des} and r^{des}. The control variables are the control surface deflections denoted

as $\mathbf{u}^{des}$ (δ_a^{des}, δ_e^{des} and δ_r^{des}). As mentioned, there are also model uncertainties in this control loop. Therefore, this loop also has to be designed based on the incremental control approach.

As done in the flight path control loop, Eq. (15) can be rewritten into the following incremental form:

$$\dot{\mathbf{x}}_3 = \dot{\mathbf{x}}_{3,0} + \mathbf{G}_3 \Delta \mathbf{u} \tag{51}$$

with

$$\dot{\mathbf{x}}_{3,0} = \mathbf{f}_{3,0} + \mathbf{G}_3 \mathbf{u}_0 \tag{52}$$

where

$$\dot{\mathbf{x}}_{3,0} = \begin{bmatrix} \dot{p}_0 \\ \dot{q}_0 \\ \dot{r}_0 \end{bmatrix}, \mathbf{u}_0 = \begin{bmatrix} \delta_{a,0} \\ \delta_{e,0} \\ \delta_{r,0} \end{bmatrix} \tag{53}$$

$\dot{\mathbf{x}}_{3,0}$ denotes the derivatives of $\mathbf{x}_3$ in the previous time step. $\mathbf{f}_{3,0}$ and $\mathbf{u}_0$ denotes $\mathbf{f}_3$ and $\mathbf{u}$ in the previous time step. The calculation of $\dot{\mathbf{x}}_{3,0}$ can be done in the same way as that of $\dot{\tilde{\mathbf{x}}}_{1,0}$ through the use of (49).

Now the desired incremental control law can be presented as follows (See Appendix C in [36] for the design principle of INDI):

$$\Delta \mathbf{u}^{des} = \begin{bmatrix} \Delta\delta_a^{des} \\ \Delta\delta_e^{des} \\ \Delta\delta_r^{des} \end{bmatrix} = \mathbf{G}_3^{-1} \Bigg(\begin{bmatrix} \nu_p \\ \nu_q \\ \nu_r \end{bmatrix} - \begin{bmatrix} \dot{p}_0 \\ \dot{q}_0 \\ \dot{r}_0 \end{bmatrix} \Bigg) \tag{54}$$

where ν_p, ν_q and ν_r are virtual controls designed based on the errors between p^{des}, q^{des}, r^{des} and p, q, r.

The final desired control law $\mathbf{u}^{des}$ is computed as follows:

$$\begin{bmatrix} \delta_a^{des} \\ \delta_e^{des} \\ \delta_r^{des} \end{bmatrix} = \begin{bmatrix} \delta_{a,0} \\ \delta_{e,0} \\ \delta_{r,0} \end{bmatrix} + \begin{bmatrix} \Delta\delta_a^{des} \\ \Delta\delta_e^{des} \\ \Delta\delta_r^{des} \end{bmatrix} \tag{55}$$

The block diagram of the angular rate control loop is shown in Fig. 4. In the figure, $\mathbf{u}^{exp}$ are the expected control surface deflections and will be discussed in more details in Section 5.

4.5. Control structure

The block diagram of the control loops is given in Fig. 5. In the figure, the reference commands and the desired reference commands generated by each control loop are shown. The performance of this trajectory controller will be demonstrated in the following sections.

5. Aircraft model and baseline controller

In this section, the aircraft model, the actuators and the control allocation scheme are introduced first in Section 5.1. In Section 5.2, the baseline controller, which is propose in [16], is briefly introduced.

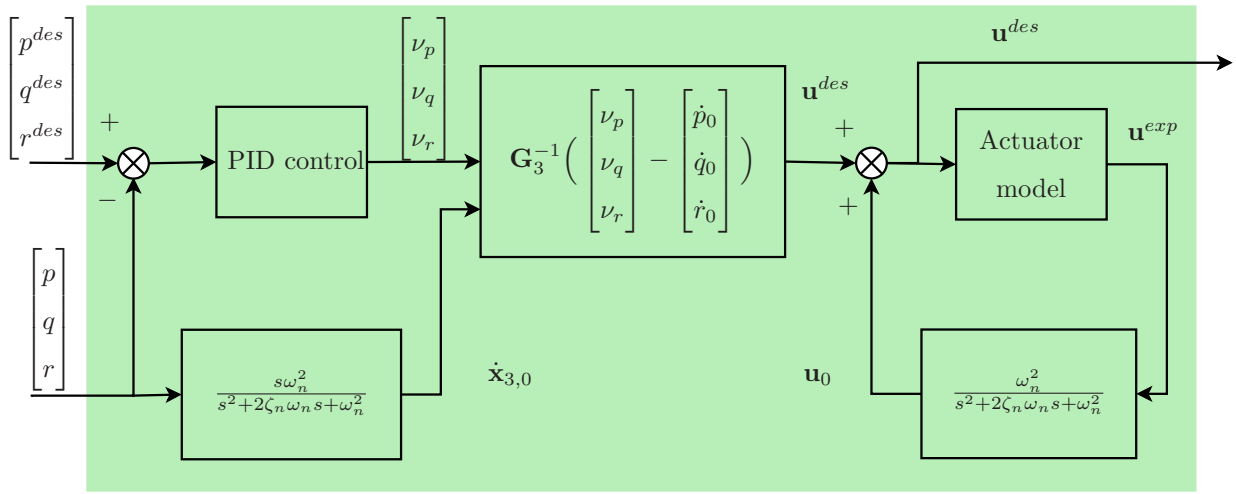

Figure 4: Block diagram of the angular rate control loop

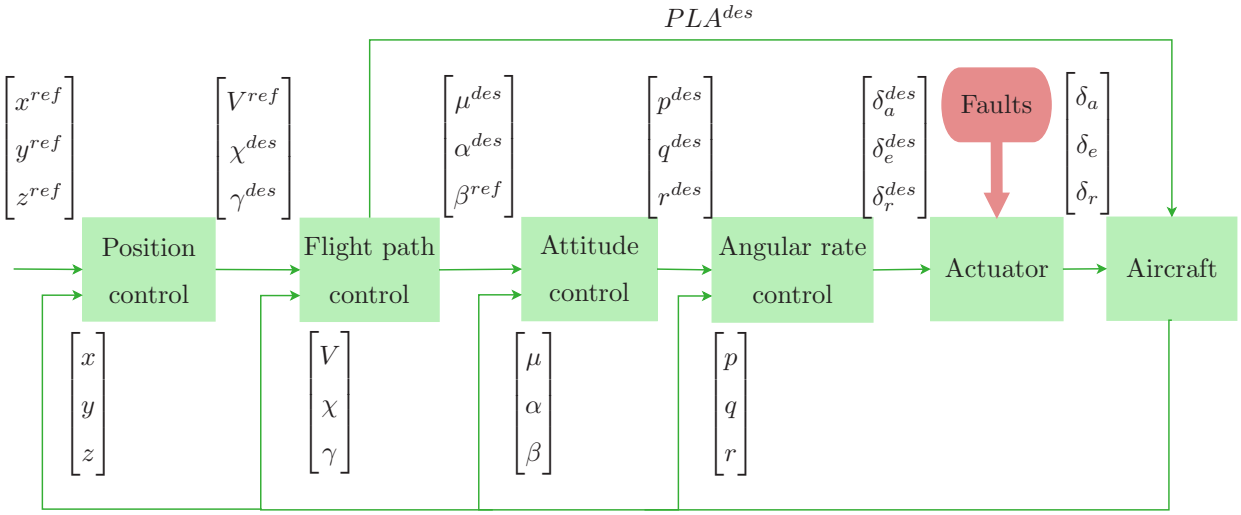

Figure 5: Block diagram of the proposed trajectory controller

5.1. Aircraft model and control allocation

The aircraft model used is the Cessna Citation aircraft [40] shown in Fig. 1. The actuator dynamics are modeled as first-order low-pass filters $1/(\tau s + 1)$. The parameter τ and the position limits of the actuators are given in Table 1. There are two engines onboard the aircraft. The thrust is controlled by the throttle (power level angle). The power level angle is within $[0.2356, 1.0820]$ rad.

Table 1: Time constants and position limits of the actuators

Actuator	$1/\tau$	Minimum position limit	Maximum position limit	Unit
elevator	13	-0.35	0.26	[rad]
aileron (left/right)	13	-0.65	0.65	[rad]
rudder (upper/lower)	13	-0.38	0.38	[rad]

For reconfiguring the controller, the left and right ailerons are assumed to be actuated by independent actuation systems such that they can deflect independently. Furthermore, the rudder is split into an upper part and a lower part in a way such that the effectiveness of these two parts are the same. Such a configuration is also considered in other papers such as [41, 42].

The positive deflections are defined in the conventional way. For example, positive δ_a means the left aileron deflects upwards and the right aileron deflects downwards.

Although there are two independent rudders and two independent ailerons, the controller design does not consider them as independent. Since the control surface commands computed by the INDI controller are $[\delta_a^{des}, \delta_e^{des}, \delta_r^{des}]^T$, the desired commands of the two rudders and two ailerons are as follows:

$$\delta_{al}^{des} = \delta_{ar}^{des} = \delta_a^{des} \tag{56}$$

$$\delta_{ru}^{des} = \delta_{rl}^{des} = \delta_r^{des} \tag{57}$$

where δ_{al}^{des}, δ_{ar}^{des}, δ_{ru}^{des} and δ_{rl}^{des} denote the commands for the left aileron, right aileron, upper rudder and lower rudder, respectively. Take the upper rudder for example, even if it is stuck, the command generated for its deflection is still δ_r^{des}. The effectiveness of the control surface pairs are assumed to be the same such that the parameters in Eq. (14) can be denoted as:

$$C_{l\delta_a} = C_{l\delta_{al}} + C_{l\delta_{ar}} = 2C_{l\delta_{al}} \tag{58}$$

$$C_{l\delta_r} = C_{l\delta_{ru}} + C_{l\delta_{rl}} = 2C_{l\delta_{ru}} \tag{59}$$

$$C_{n\delta_a} = C_{n\delta_{al}} + C_{n\delta_{ar}} = 2C_{n\delta_{al}} \tag{60}$$

$$C_{n\delta_r} = C_{n\delta_{ru}} + C_{n\delta_{rl}} = 2C_{n\delta_{ru}} \tag{61}$$

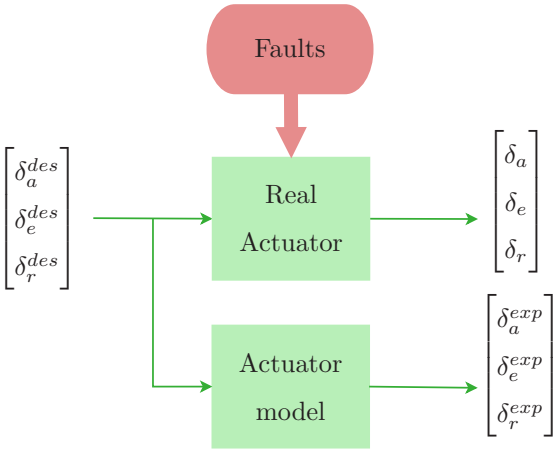

Figure 6: True and expected actuator deflections

5.2. Baseline control approach: NDI-MI

In this section, a baseline control approach used for comparison, NDI-MI [16], is briefly introduced. The NDI-MI uses Eq. (5) for flight path control and Eq. (15) for angular rate control while the INDI uses Eq. (45) for flight path control and Eq. (51) for angular rate control. The core of the NDI-MI is to identify the unknown parameters online to reduce the model uncertainty. Take the lateral motion for example, the lateral force and moments are assumed to be expressed as follows:

$$Y = \bar{q}SC_y = \bar{q}S(C_{y_0} + C_{y_\beta}\beta + C_{y_p}\frac{pb}{2V} + C_{y_r}\frac{rb}{2V} + C_{y_{\delta_a}}\delta_a^{exp} + C_{y_{\delta_r}}\delta_r^{exp}) \tag{62}$$

$$L = \bar{q}SC_l = \bar{q}S(C_{l_0} + C_{l_\beta}\beta + C_{l_p}\frac{pb}{2V} + C_{l_r}\frac{rb}{2V} + C_{l_{\delta_a}}\delta_a^{exp} + C_{l_{\delta_r}}\delta_r^{exp}) \tag{63}$$

$$N = \bar{q}SC_n = \bar{q}S(C_{n_0} + C_{n_\beta}\beta + C_{n_p}\frac{pb}{2V} + C_{n_r}\frac{rb}{2V} + C_{n_{\delta_a}}\delta_a^{exp} + C_{n_{\delta_r}}\delta_r^{exp}) \tag{64}$$

where δ_a^{exp} and δ_r^{exp}, which can be obtained using the actuator model as shown in Fig. 6, denote the expected actuator deflections. The NDI-MI also treats the control surface pairs as one control surface. For instance, it does not identify $C_{l\delta_{al}}$ and $C_{l\delta_{ar}}$, but only identifies $C_{l\delta_a}$. The aerodynamic model structure in Eqs. (62)-(64) is a simplified structure. To deal with aircraft dynamics with significant nonlinearities, a more complex structure should be designed [22, 14]. However, this is not required if the proposed approach, which uses the INDI, is used. The differences between δ_a^{exp}, δ_e^{exp}, δ_r^{exp} and δ_a, δ_e, δ_r are shown in Fig. 6. It is seen that the expected deflections δ_a^{exp}, δ_e^{exp}, δ_r^{exp} are free from the influence of faults.

First, the lateral force coefficient C_y and lateral moment coefficients C_l and C_n are calculated [16]. Then the parameters can be identified using parameter estimation methods such as the recursive least squares

method [16]. The identified parameters are denoted as:

$$\hat{C}_{y_0}, \hat{C}_{y_\beta}, \hat{C}_{y_p}, \hat{C}_{y_r}, \hat{C}_{y_{\delta_a}}, \hat{C}_{y_{\delta_r}} \tag{65}$$

$$\hat{C}_{l_0}, \hat{C}_{l_\beta}, \hat{C}_{l_p}, \hat{C}_{l_r}, \hat{C}_{l_{\delta_a}}, \hat{C}_{l_{\delta_r}} \tag{66}$$

$$\hat{C}_{n_0}, \hat{C}_{n_\beta}, \hat{C}_{n_p}, \hat{C}_{n_r}, \hat{C}_{n_{\delta_a}}, \hat{C}_{n_{\delta_r}} \tag{67}$$

When an actuator fault occurs, the above parameters can change due to the difference between the true and expected actuator deflections. In this case, the parameter estimation process needs to be re-initialized in order to identify the change of the parameters. The re-initialization is triggered by statistics monitoring [16]. Define

$$M_{lat} = \frac{1}{N_w} \sum_{i=0}^{N_w} (\Delta C_{y,i}^2 + \Delta C_{l,i}^2 + \Delta C_{n,i}^2) \tag{68}$$

where N_w is a pre-selected size of a moving window and

$$\Delta C_{y,i} = C_y - (\hat{C}_{y_0} + \hat{C}_{y_\beta}\beta + \hat{C}_{y_p}\frac{pb}{2V} + \hat{C}_{y_r}\frac{rb}{2V} + \hat{C}_{y_{\delta_a}}\delta_a^{exp} + \hat{C}_{y_{\delta_r}}\delta_r^{exp}) \tag{69}$$

$$\Delta C_{l,i} = C_l - (\hat{C}_{l_0} + \hat{C}_{l_\beta}\beta + \hat{C}_{l_p}\frac{pb}{2V} + \hat{C}_{l_r}\frac{rb}{2V} + \hat{C}_{l_{\delta_a}}\delta_a^{exp} + \hat{C}_{l_{\delta_r}}\delta_r^{exp}) \tag{70}$$

$$\Delta C_{n,i} = C_n - (\hat{C}_{n_0} + \hat{C}_{n_\beta}\beta + \hat{C}_{n_p}\frac{pb}{2V} + \hat{C}_{n_r}\frac{rb}{2V} + \hat{C}_{n_{\delta_a}}\delta_a^{exp} + \hat{C}_{n_{\delta_r}}\delta_r^{exp}) \tag{71}$$

The parameter estimation needs to be re-initialized when the following is satisfied:

$$M_{lat} > T_{M_{lat}} \tag{72}$$

where $T_{M_{lat}}$ is the threshold to trigger the re-initialization of the parameter identification. Furthermore, define the following difference between the real values of C_y, C_l, C_n and the estimated ones using the NDI-MI as follows:

$$\Delta C_y = C_{y,real} - (\hat{C}_{y_0} + \hat{C}_{y_\beta}\beta + \hat{C}_{y_p}\frac{pb}{2V} + \hat{C}_{y_r}\frac{rb}{2V} + \hat{C}_{y_{\delta_a}}\delta_a^{exp} + \hat{C}_{y_{\delta_r}}\delta_r^{exp}) \tag{73}$$

$$\Delta C_l = C_{l,real} - (\hat{C}_{l_0} + \hat{C}_{l_\beta}\beta + \hat{C}_{l_p}\frac{pb}{2V} + \hat{C}_{l_r}\frac{rb}{2V} + \hat{C}_{l_{\delta_a}}\delta_a^{exp} + \hat{C}_{l_{\delta_r}}\delta_r^{exp}) \tag{74}$$

$$\Delta C_n = C_{n,real} - (\hat{C}_{n_0} + \hat{C}_{n_\beta}\beta + \hat{C}_{n_p}\frac{pb}{2V} + \hat{C}_{n_r}\frac{rb}{2V} + \hat{C}_{n_{\delta_a}}\delta_a^{exp} + \hat{C}_{n_{\delta_r}}\delta_r^{exp}) \tag{75}$$

where $C_{y,real}$, $C_{l,real}$, $C_{n,real}$ are the real values of C_y, C_l and C_n, which is obtained from the Citation model [40]. ΔC_y, ΔC_l and ΔC_n can be used to evaluate the identification performance of the NDI-MI [21].

Similarly, the re-initialization of the parameter identification for the longitudinal motion is triggered when

$$M_{long} > T_{M_{long}} \tag{76}$$

where M_{long} and $T_{M_{long}}$ are defined the same way as M_{lat} and $T_{M_{lat}}$. $T_{M_{long}}$ is the threshold to trigger the re-initialization of the parameter identification. ΔC_x, ΔC_z and ΔC_m are defined to denote the differences between the real values of C_x, C_z, C_m and the estimated values using the NDI-MI.

A comparison of NDI-MI with the proposed approach will be demonstrated in the following section. **Remark:** Since the NDI-MI uses Eqs. (5) and (15), it requires the aerodynamic model structure (described by Eqs. (62), (63) and (64)). This aerodynamic model structure can change during the whole flight envelope [15]. It also changes when there are actuator faults. Consequently, the performance of the NDI-MI degrades when the aerodynamic model structure is not accurate. However, the proposed method using the INDI is less sensitive to the the aerodynamic model structure since it does not require the complete aerodynamic model as can be seen in Eq. (45) and (51).

6. Performance validation results

In this section, the performance of the trajectory controller using the INDI will be demonstrated. The trajectory reference in three-dimensional space is given in Fig 7(a). x^{ref}, y^{ref} and z^{ref} are given in Fig. 7(b). Besides, $V^{ref} = 90$ m/s and $\beta^{ref} = 0$ rad. This means that the aircraft should fly at a constant speed and perform coordinated turns.

To demonstrate the performance of the proposed trajectory controller, the NDI-MI is also applied to control the trajectory of the aircraft. The control gains of the four loops used for both controllers are given in Table 2. In the table, K_P, K_I and K_D are the PID gains for each loop.

Table 2: Control gains for four loops

Gains	Position	Flight path	Attitude	Angular rate
K_P	1	1.5	2.5	5
K_I	0.01	0.01	0.5	0.5
K_D	0.05	0.05	0.5	0.5

The initial states of the aircraft is:

$$z = -2000 \text{ m}, \ \gamma = -3\pi/180 \text{ rad},$$
$$V = 90 \text{ m/s}, \quad \alpha = 3.2\pi/180 \text{ rad}$$

Other states are close to zero and are not shown. In Section 6.1, the actuator fault scenario is introduced. The performance of the proposed trajectory controller with the one using the NDI-MI is compared under three scenarios which is presented in Sections 6.2, 6.3 and 6.4.

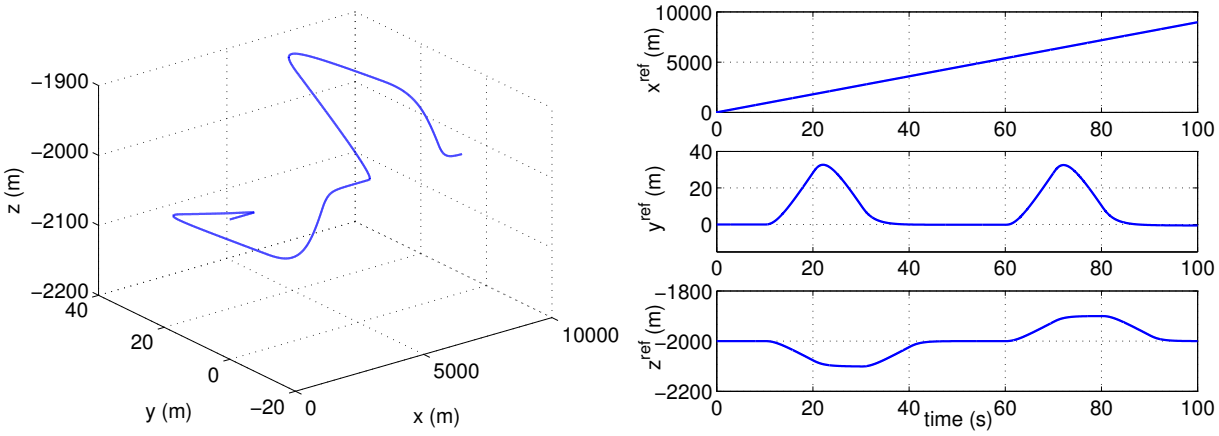

(a) Trajectory reference in three-dimensional space

(b) x^{ref}, y^{ref} and z^{ref}

Figure 7: Results of aircraft trajectory control without faults

6.1. Actuator fault scenario and modeling of the faults

In this section, the modeling of the actuator faults are presented.

The actuator faults considered in this paper are jamming faults where the control surfaces are stuck at a certain position. The specific fault occurrence time and stuck position is given in Table 3.

Table 3: Actuator faults

Time interval	Actuator	Fault type	Stuck position	Fault unit
$t > 25$ s	left aileron	Jamming	0.56	[rad]
$t > 50$ s	upper rudder	Jamming	0.2	[rad]

It can be seen that during 25 s $< t \leq$ 100 s, the left aileron is stuck. During 50 s $< t \leq$ 100 s, the left aileron and the upper rudder both fail. Therefore, simultaneous actuator faults are taken into account in this paper.

6.2. Validation in the absence of faults

In this section, the performance of trajectory control using the NDI-MI and the INDI is compared. In this section, there are no actuator faults.

Both controller require initial values for the aerodynamic parameters (control and stability derivatives). For the INDI, once the initial parameters are given, they are considered fixed during the whole flight. For the NDI-MI, although it requires initial parameters, the initial parameters will be changed due to the on-line model identification. This scenario is to test the performance of the controllers in a nominal situation when

there are no model uncertainties and faults. Therefore, the initial parameters given to the controllers are both the real parameters of the aircraft at the initial condition.

Results of using the NDI-MI

The trajectory control results using the NDI-MI are shown in Fig. 8. As can be seen from Fig. 8(a), the trajectory can follow the reference. The true and desired V, χ and γ are shown in Fig. 8(b). As can be seen, the response is satisfactory. The velocity is kept within 85-95 m/s. This is acceptable since the engine of the aircraft is not as powerful as a fighter. The engine power level angles are shown in Fig. 8(c). It is seen that saturations are observed. The fluctuations in the beginning of γ response is caused by the fact that the initial γ is not zero and the aircraft needs to reach a new equilibrium to hold the altitude.

The control inputs are presented. Fig. 8(c) shows PLA_1 and PLA_2. The control surface deflections δ_{ar}, δ_e and δ_{rl} are shown in Fig. 8(d). The control surface deflections δ_{al} and δ_{ru} are the same as δ_{ar} and δ_{rl} respectively and are therefore not shown.

The differences between the real C_x, C_y, C_z, C_l, C_m, C_n and their estimates using the NDI-MI are shown in Figs. 8(e) and 8(f) respectively. It is seen that all the differences are close to zero-mean, which indicates that the performance of the on-line model identification is satisfactory. This performance can be further improved by the re-identification, which is introduced in the following section.

Results of using the INDI

The trajectory control results using the INDI are shown in Fig. 9. It is seen from Fig. 9(a) that the trajectory can follow the reference. The tracking performance is satisfactory. V, χ and γ can follow the desired reference generated by the position control loop, as shown in Fig. 9(b).

The attitude response using the INDI is shown in Fig. 9(c). μ, α can follow their desired references and β is smaller than 0.2 deg. The desired references for p, q and r are shown in Fig. 9(d). It is seen that the references are tracked well and no oscillations are observed.

Finally, the control inputs using the INDI are shown in Fig. 9(e) and 9(f). It is seen from Fig. 9(e) that PLA_1 and PLA_2 also reach their limits. The deflections δ_{ar}, δ_e and δ_{rl} are shown in Fig. 9(f). It is seen that no oscillations are present. Control surface deflections δ_{al} and δ_{ru} are the same as δ_{ar} and δ_{rl} respectively and are therefore not shown.

Comparison in the absence of faults

In this scenario, the performance of both the INDI and NDI-MI is satisfactory. The RMSEs of the tracking errors of x, y, z are shown in Fig. 10. It is seen that the RMSEs of both controllers are close, especially the RMSEs of y and z.

6.3. Validation in the presence of uncertainties

In this scenario, the initial parameters given to the two controllers are modified to generate model uncertainties. Then these parameters with model uncertainties will be given to the controllers to test the performance of the controllers in the presence of model uncertainties. It should be noted that the model uncertainties can also be viewed as the results of structural faults.

Persistent excitation is important in system identification. Although the requirement of persistent excitation is weaker using the NDI-MI [16], excitation is still needed in order to identify the derivatives. To ensure proper identification, a trigger for re-identification is required. To trigger the re-identification, thresholds ($T_{M_{long}}$ and $T_{M_{lat}}$) have to be chosen.

Results of using the NDI-MI

First of all, all the parameters are multiplied by 80%. The result using the NDI-MI are shown in Fig. 11.

The trajectory of the aircraft is shown in Fig. 11(a). It is seen that the aircraft trajectory can follow the reference well despite the model uncertainties. The control inputs are shown in Fig. 11(b). No saturations are observed from the figure.

The reason why the NDI-MI worked in the presence of model uncertainties is due to the triggered re-identification. To trigger the re-identification, choosing the thresholds is critical. If the threshold is "large", it could lead to failure of the model identification (this will be demonstrated later on). In this case, the following thresholds are chosen:

$$T_{M_{long}} = 0.003,\ T_{M_{lat}} = 9 \times 10^{-4} \tag{77}$$

M_{long} and M_{lat} together with the thresholds using the NDI-MI are shown in Fig. 11(c). It is seen that both M_{long} and M_{lat} exceed their thresholds and triggered the re-identification. The re-identified parameters are shown in Fig. 11(d).

To further evaluate the performance of the NDI-MI, the differences between the real C_x, C_y, C_z, C_l, C_m, C_n and their estimation using the NDI-MI are shown in Figs. 11(e) and 11(f) respectively. It is seen that all the differences are zero-mean, which indicates that the performance of the on-line model identification is satisfactory.

In the following, the performance of the NDI-MI, when different thresholds are chosen, is demonstrated. The thresholds are slightly increased as follows:

$$T_{M_{long}} = 0.004,\ T_{M_{lat}} = 1.25 \times 10^{-3} \tag{78}$$

The results of using the NDI-MI are shown in Fig. 12. In this case, M_{long} and M_{lat} together with the thresholds using the NDI-MI are shown in Fig. 12(c). It is seen that the thresholds are not exceeded until after $t = 62$ s. In the first 60 s, the aircraft can still follow the trajectory reference, as shown in Fig.12(a).

However, it can be seen from the control surface deflections (Fig.12(b)) that after $t = 10$ s, significant oscillations are observed. This is caused by the model uncertainties. After $t = 10$ s, there are longitudinal and lateral maneuvers and the aerodynamic parameters can further change due to the change of the flight condition. Although the parameters are identified on-line, without the re-identification, convergence of parameter estimation is not guaranteed. Consequently, incorrect estimated parameters (shown in Fig. 12(d)) lead to the oscillations of the control surfaces.

The differences between the real C_x, C_y, C_z, C_l, C_m, C_n and their estimated values using the NDI-MI, when there are no re-identification, are shown in Figs. 12(e) and 12(f). As can be seen from the figures, the differences are no longer zero-mean, which confirms that the estimated parameters are not correct.

The results when different thresholds are chosen demonstrate the importance of choosing a reasonable threshold. Further simulations indicate that when the parameters are multiplied with different constants, different thresholds should be chosen in order to trigger the re-identification. However, there are no rules for choosing the thresholds.

In the next, the model uncertainties are increased. All the parameters are multiplied with 50%. In this case, the aircraft is no longer able to follow the trajectory even when the parameter re-identification is triggered and the simulation is terminated around $t = 5.7$ s, as shown in Fig. 13(a). The control surface deflections are shown in Fig. 13(b). It is seen from the figure that the elevator reaches its position limit.

Results of using the INDI

In contrast, the performances of using the INDI, when all the parameters are multiplied with 80% and 50% respectively, are similar as the case when there is no model uncertainty and the results are not shown. This also demonstrates the benefits of the INDI. Its performance is still satisfactory when there are model uncertainties.

Comparison in the presence of model uncertainties

In this section, the performance of both controllers when there are model uncertainties is compared. It is shown that the performance of the controller using the NDI-MI depends on the chosen thresholds. The controller using the INDI does not require a threshold. When the initial parameters are multiplied with 80%, the performances of both controllers are similar. When the parameters are multiplied with 50%, the controller using the NDI-MI can no longer follow the reference whereas that using the INDI can still follow the reference well. This demonstrates one benefit of using the INDI: it does not require choosing a threshold.

6.4. Validation in the presence of actuator faults

In this final scenario, a more challenging problem is considered. The model uncertainties are included in the parameters by multiplying each parameter with 50%. In addition, the actuators faults, which are given

in Table 3, are also considered. Since the NDI-MI does not work when the parameters are all multiplied with 50%, its performance is not shown in this section.

The results using the INDI are shown in Fig. 14. No significant difference between the trajectory and its reference is found in Fig. 14(a). Its performance is comparable with the scenario when there are no faults or model uncertainties. However, slight differences and performance degradation can still be observed. At $t = 25$ s and $t = 50$ s, χ, μ are influenced by the faults, as can be seen from Figs. 14(b) and 14(c). Especially, β is influenced. Two peaks are generated due to the faults. β, which is around 0.1 deg when there are no faults, reaches 0.6 deg in this scenario. p and r are also influenced and cannot follow their references well when the faults occur, as observed from Fig. 14(d).

The control surface deflections δ_{al} and δ_{ru} are shown in Fig. 14(e). It is seen that they are stuck at $t = 25$ s and $t = 50$ s respectively. The control surface deflections δ_{ar}, δ_e and δ_{rl}, which provide the remaining control authority for reconfiguration, are shown in Fig. 14(f). In order to compensate the influence of the faults, δ_{ar} and δ_{rl} are controlled to deflect opposite angles of which δ_{al} and δ_{ru} are stuck at.

7. Conclusions

This paper proposes an aircraft fault-tolerant trajectory controller. The nonlinearities in the aircraft model are dealt with using a Nonlinear Dynamic Inversion (NDI) approach. The uncertainties in the aircraft model are treated by the Incremental Nonlinear Dynamic Inversion (INDI) approach. The trajectory controller is split into four control loops: position control, flight path control, attitude control and angular rate control. The detailed control law of the flight path control and the angular rate control loop, which use the INDI approach, are presented in the paper. The other two loops, position control and attitude control loops are designed based on the standard NDI approach.

The performance of the proposed trajectory controller is compared to an existing control approach which is Nonlinear Dynamic Inversion with model identification (NDI-MI). Their performances are compared using three scenarios. The drawback of the NDI-MI is that it requires excitation and a selection of thresholds. The results of the comparison demonstrate the superior performance of the proposed controller which does not require sufficient excitation and choosing thresholds. Therefore, the proposed controller is more robust to model uncertainties in increasing the safety of the aircraft in the presence of actuator faults.

In the future, an experiment of the proposed approach on a fixed-wing unmanned aerial vehicle is highly recommended. Through doing this, the performance of the proposed approach can be validated under real-life model uncertainties and fault scenarios.

Reference

[1] I. Kaminer, A. Pascoal, E. Hallberg, C. Silvestre, Trajectory Tracking for Autonomous Vehicles : An Integrated Approach to Guidance and Control, Journal of Guidance, Control, and Dynamics 21 (1998) 29–38.

[2] R. J. Patton, Fault-tolerant Control Systems: The 1997 Situation, in: Proc. of IFAC Symp. on Fault Detection, Supervision and Safety for Technical Processes, 1997, pp. 1033–1054.

[3] Y. Zhang, J. Jiang, Bibliographical review on reconfigurable fault-tolerant control systems, Annual reviews in control (2008) 229–252.

[4] A. Zolghadri, Advanced model-based fdir techniques for aerospace systems: Today challenges and opportunities, Progress in Aerospace Sciences 53 (2012) 18–29.

[5] A. Zolghadri, D. Henry, J. Cieslak, D. Efimov, P. Goupil, Fault Diagnosis and Fault-Tolerant Control and Guidance for Aerospace Vehicles, from theory to application, Springer, Series: Advances in Industrial Control, 2013.

[6] F. A. D. Almeida, D. Leiß ling, Fault-Tolerant Model Predictive Control with Flight-Test Results, Journal of Guidance, Control, and Dynamics 33 (2010).

[7] G.-h. Yang, J. L. Wang, Y. C. Soh, Reliable H infinity controller design for linear systems, Automatica 37 (2001) 717–725.

[8] Y. Shtessel, J. Buffington, S. Banda, Tailless Aircraft Flight Control Using Multiple Time Scale Reconfigurable Sliding Modes, IEEE Transactions on Control Systems Technology 10 (2002) 288–296.

[9] H. Alwi, C. Edwards, O. Stroosma, J. A. Mulder, Evaluation of a Sliding Mode Fault-Tolerant Controller for the El Al Incident, Journal of Guidance, Control, and Dynamics 33 (2010) 677–694.

[10] V. Dobrokhodov, I. Kaminer, I. Kitsios, E. Xargay, N. Hovakimyan, C. Cao, I. M. Gregory, L. Valavani, Experimental Validation of L1 Adaptive Control: The Rohrs Counterexample in Flight, Journal of Guidance, Control, and Dynamics 34 (2011) 1311–1328.

[11] P. Castaldi, N. Mimmo, S. Simani, Differential geometry based active fault tolerant control for aircraft, Control Engineering Practice 32 (2014) 227–235.

[12] S. N. Singh, M. L. Steinberg, A. B. Page, Nonlinear Adaptive and Sliding Mode Flight Path Control of F / A-18 Model, IEEE Transactions on Aerospace and Electronic Systems 39 (2003) 1250–1262.

[13] W. Ren, R. W. Beard, Trajectory Tracking for Unmanned Air Vehicles With Velocity and Heading Rate Constraints, IEEE Transactions on Control Systems Technology 12 (2004) 706–716.

[14] J. Farrell, M. Sharma, M. Polycarpou, Backstepping-Based Flight Control with Adaptive Function Approximation, Journal of Guidance, Control, and Dynamics 28 (2005) 1089–1102.

[15] L. Sonneveldt, E. R. Van Oort, Q. P. Chu, J. A. Mulder, Nonlinear Adaptive Trajectory Control Applied to an F-16 Model, Journal of Guidance, Control, and Dynamics 32 (2009) 25–39.

[16] T. J. J. Lombaerts, Q. P. Chu, J. A. Mulder, D. A. Joosten, Modular flight control reconfiguration design and simulation, Control Engineering Practice 19 (2011) 540–554.

[17] M. Maximilian, J. C. Dauer, F. Holzapfel, Adaptive Trajectory Controller for Generic Fixed-Wing Unmanned Aircraft, in: Proceedings of the EuroGNC 2013, 2nd CEAS Special Conference on Guidance, Navigation & Control, 2013, pp. 236–255.

[18] M. Krstić, I. Kanellakopoulos, P. Kokotović, Adaptive nonlinear control without overparametrization, Systems & Control Letters 19 (1992) 177–185.

[19] M. Krstic, I. Kanellakopoulos, P. Kokotovic, Nonlinear and Adaptive Control Design, John Wiley & Sons, Inc., 1995.

[20] L. Sonneveldt, Q. P. Chu, J. A. Mulder, Nonlinear Flight Control Design Using Constrained Adaptive Backstepping, Journal of Guidance, Control, and Dynamics 30 (2007).

[21] H. J. Tol, C. C. D. Visser, L. G. Sun, E. V. Kampen, Q. P. Chu, Multivariate Spline-Based Adaptive Control of High-Performance Aircraft with Aerodynamic Uncertainties, Journal of Guidance, Control and Dynamics (2016) 1–20 (in press).

[22] T. J. J. Lombaerts, E. R. Van Oort, Q. P. Chu, J. A. Mulder, D. A. Joosten, Online Aerodynamic Model Structure Selection and Parameter Estimation for Fault-Tolerant Control, Journal of Guidance, Control and Dynamics 33 (2010) 707–723.

[23] B. J. Bacon, A. J. Ostroff, S. M. Joshi, Reconfigurable NDI Controller Using Inertial Sensor Failure Detection & Isolation, IEEE Transactions on Aerospace and Electronic Systems 37 (2001) 1373–1383.

[24] S. Sieberling, Q. P. Chu, J. A. Mulder, Robust Flight Control Using Incremental Nonlinear Dynamic Inversion and Angular Acceleration Prediction, Journal of Guidance, Control, and Dynamics 33 (2010) 1732–1742.

[25] P. Simplício, M. Pavel, E. van Kampen, Q. Chu, An acceleration measurements-based approach for helicopter nonlinear flight control using Incremental Nonlinear Dynamic Inversion, Control Engineering Practice 21 (2013) 1065–1077.

[26] J. Marzat, H. Piet-Lahanier, F. Damongeot, E. Walter, Model-based fault diagnosis for aerospace systems: a survey, Proceedings of the Institution of Mechanical Engineers, Part G: Journal of Aerospace Engineering 226 (2012) 1329–1360.

[27] P. Castaldi, W. Geri, M. Bonfe, S. Simani, M. Benini, Design of residual generators and adaptive filters for the FDI of aircraft model sensors, Control Engineering Practice 18 (2010) 449–459.

[28] P. Freeman, P. Seiler, G. J. Balas, Air data system fault modeling and detection, Control Engineering Practice 21 (2013) 1290–1301.

[29] P. Lu, L. Van Eykeren, E. van Kampen, C. C. de Visser, Q. Chu, Double-model adaptive fault detection and diagnosis applied to real flight data, Control Engineering Practice 36 (2015) 39–57.

[30] P. Lu, E. van Kampen, C. de Visser, Q. Chu, Nonlinear aircraft sensor fault reconstruction in the presence of disturbances validated by real flight data, Control Engineering Practice 49 (2016) 112–128.

[31] B. L. Stevens, F. L. Lewis, Aircraft Control and Simulation, Wiley, New York, 1992.

[32] D. Mclean, Automatic Flight Control Systems, Englewood Cliffs, NJ: Prentice-Hall, 1990.

[33] J. A. Farrell, M. Polycarpou, M. Sharma, W. Dong, Command Filtering Backstepping, IEEE Transactions on Automatic Control 54 (2009) 1391–1395.

[34] W. Dong, J. A. Farrell, M. M. Polycarpou, V. Djapic, M. Sharma, Command Filtered Adaptive Backstepping, IEEE Transactions on Control Systems Technology 20 (2012) 566–580.

[35] H. K. Khalil, Nonlinear Systems Third Edition, Prentice Hall, 2002.

[36] P. Lu, Fault Diagnosis and Fault-Tolerant Control for Aircraft Subjected to Sensor and Actuator Faults, Ph.D. thesis, Delft University of Technology, 2016.

[37] P. Lu, E. van Kampen, Q. Chu, Robustness and Tuning of Incremental Backstepping, in: AIAA Guidance, Navigation and Control Conference, AIAA 2015-1762, Kissimmee, Florida, 2015, pp. 1–15.

[38] A. Levant, Robust exact differentiation via sliding mode technique, Automatica 34 (1998) 379–384.

[39] E. J. J. Smeur, Q. Chu, G. C. H. E. D. Croon, Adaptive Incremental Nonlinear Dynamic Inversion for Attitude Control of Micro Air Vehicles, Journal of Guidance, Control, and Dynamics (2016) 1–12.

[40] C. van der Linden, DASMAT-Delft University Aircraft Simulation Model and Analysis Tool, Delft University Press, 1998.

[41] R. Venkataraman, M. Lukatsi, B. Vanek, P. Seiler, Reliability Assessment Reliability Assessment of Actuator Architectures for Unmanned Aircraft, in: 9th IFAC Symposium on Fault Detection, Supervision and Safety of Technical Processes, 2015, pp. 398–403.

[42] P. Lu, E. van Kampen, Active Fault-Tolerant Control System using Incremental Backstepping Approach, in: AIAA Guidance, Navigation and Control Conference, AIAA 2015-1312, Kissimmee, Florida, 2015, pp. 1–17.

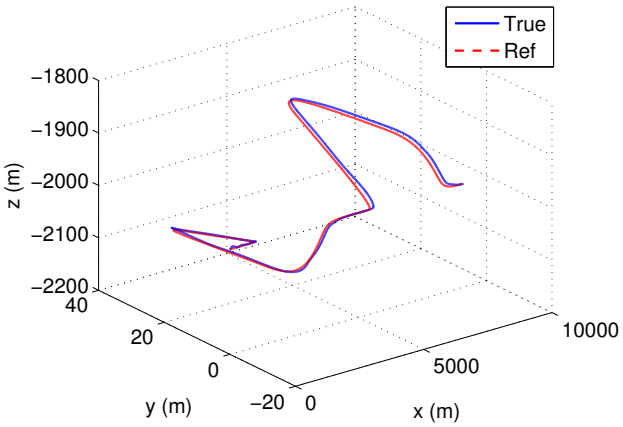

(a) Desired and true x, y and z

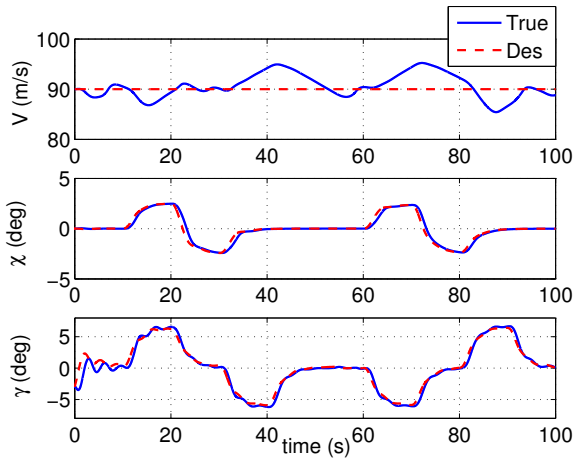

(b) Desired and true V, χ and γ

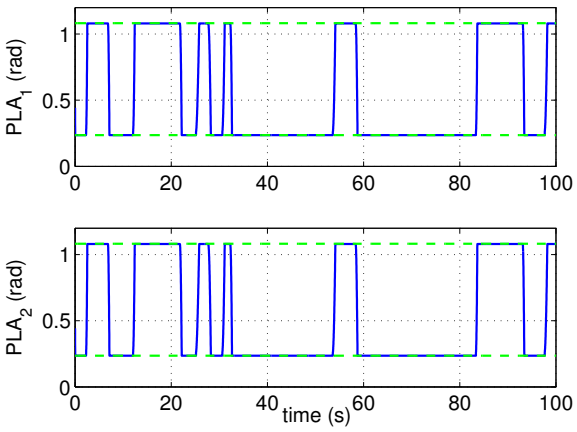

(c) PLA_1 and PLA_2, dashed lines represent the limits.

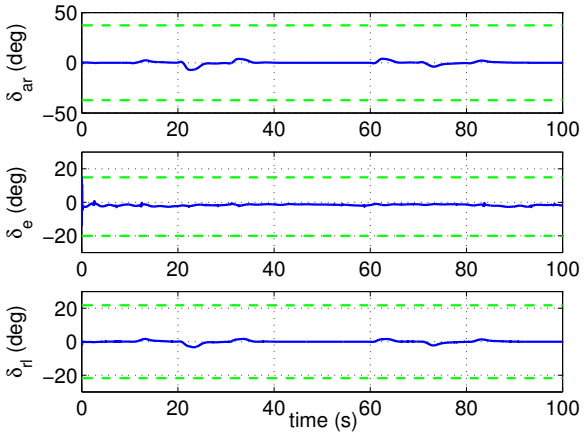

(d) δ_{ar}, δ_e and δ_{rl}, dashed lines represent the position limits.

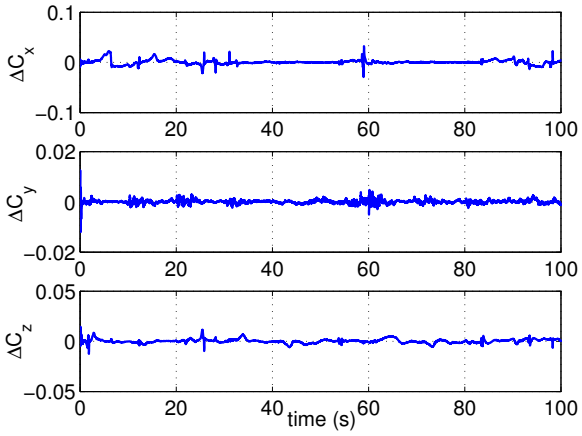

(e) ΔC_x, ΔC_y and ΔC_z

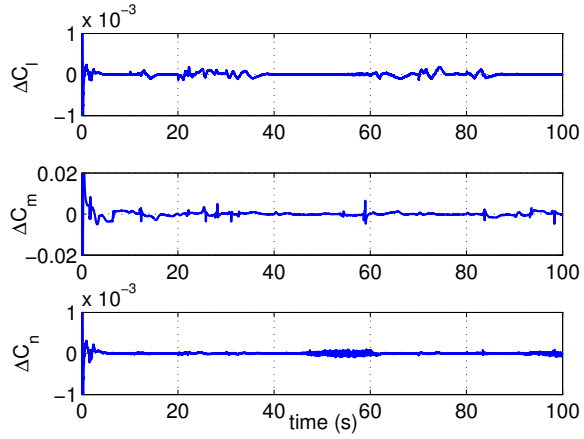

(f) ΔC_l, ΔC_m and ΔC_n

Figure 8: Results of aircraft trajectory control using the NDI-MI without faults.

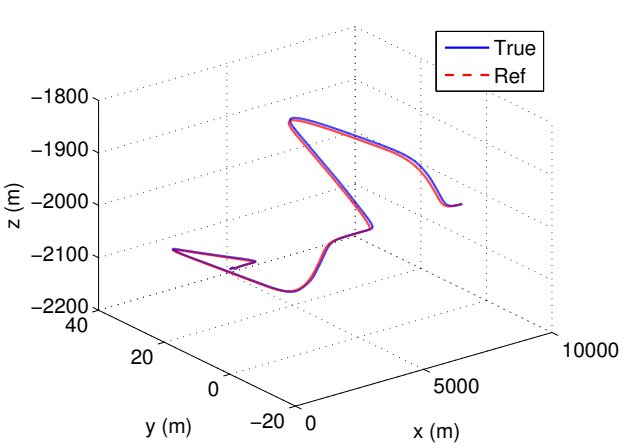

(a) Desired and true x, y and z

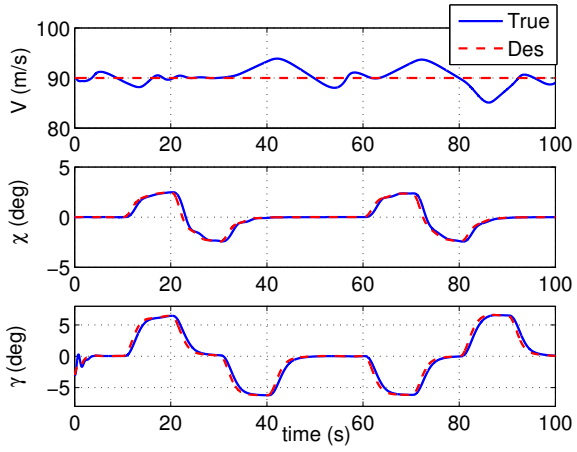

(b) Desired and true V, χ and γ

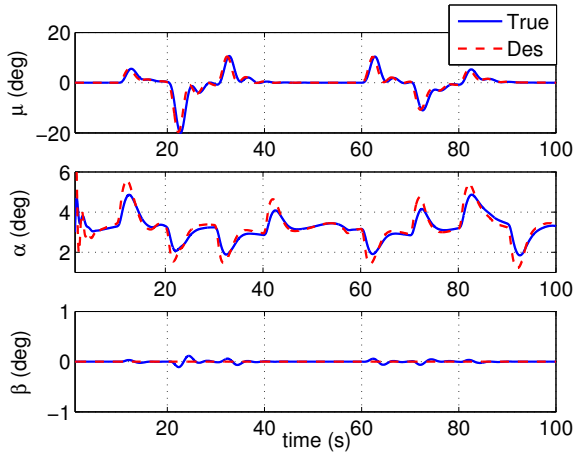

(c) Desired and true μ, α and β

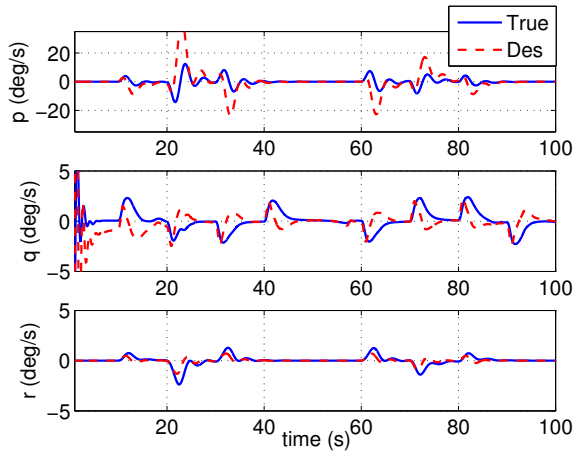

(d) Desired and true p, q and r

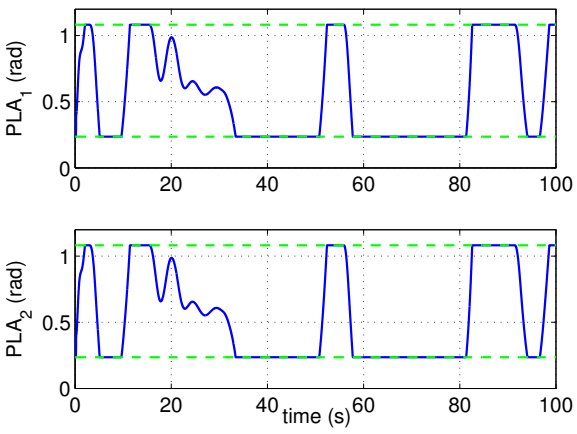

(e) PLA_1 and PLA_2, dashed lines represent the limits.

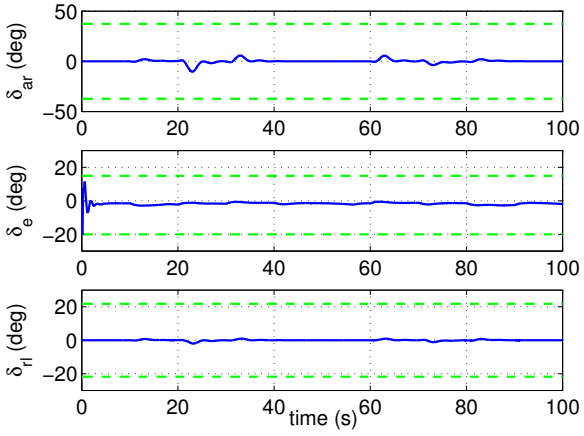

(f) δ_{ar}, δ_e and δ_{rl}, dashed lines represent the position limits.

Figure 9: Results of aircraft trajectory control using the INDI without faults

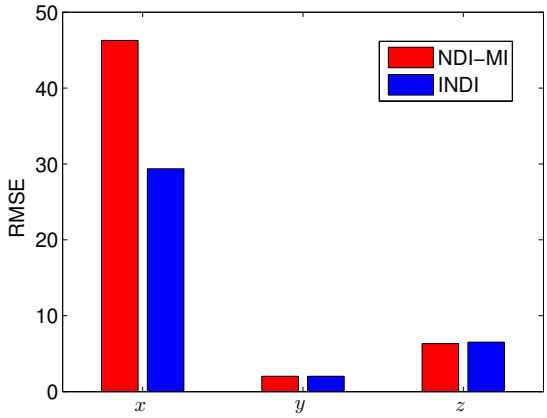

Figure 10: root mean square errors (RMSE) of x, y and z using the INDI and the NDI-MI

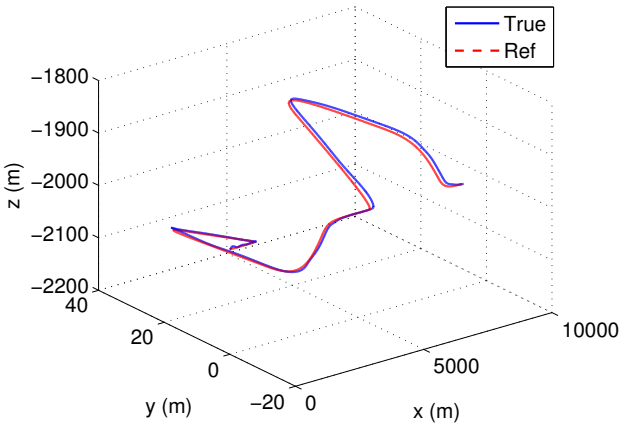

(a) Desired and true x, y and z

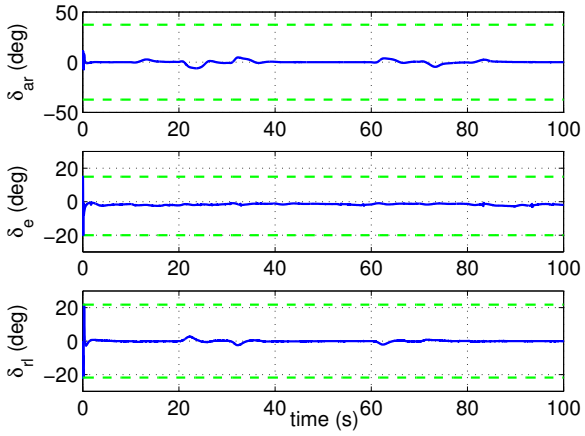

(b) δ_{ar}, δ_e and δ_{rl}, dashed lines represent the position limits.

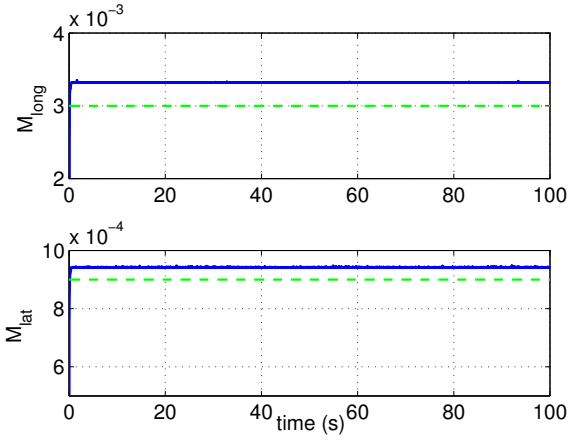

(c) M_{long} and M_{lat}, dashed lines represent the thresholds.

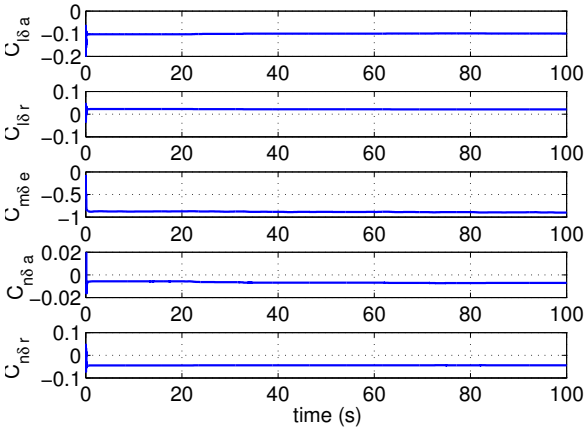

(d) Identified $C_{l\delta_a}$, $C_{l\delta_r}$, $C_{m\delta_e}$, $C_{n\delta_a}$ and $C_{n\delta_r}$

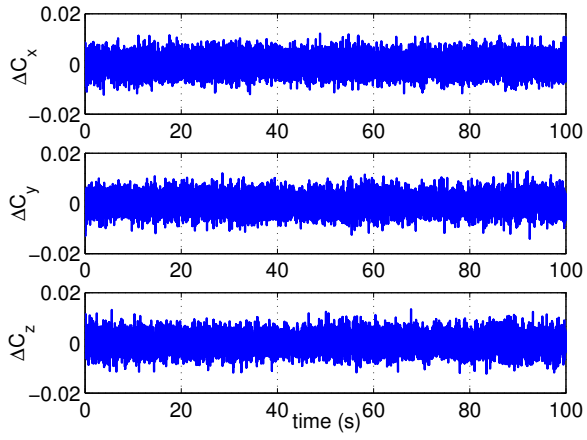

(e) ΔC_x, ΔC_y and ΔC_z

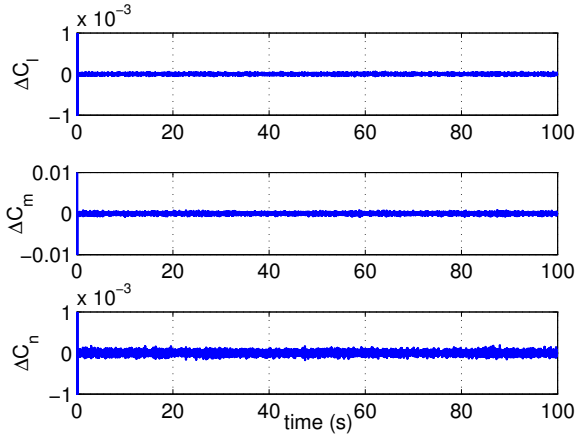

(f) ΔC_l, ΔC_m and ΔC_n

Figure 11: Results of aircraft trajectory control using the NDI-MI with thresholds (77) in the presence of model uncertainties.

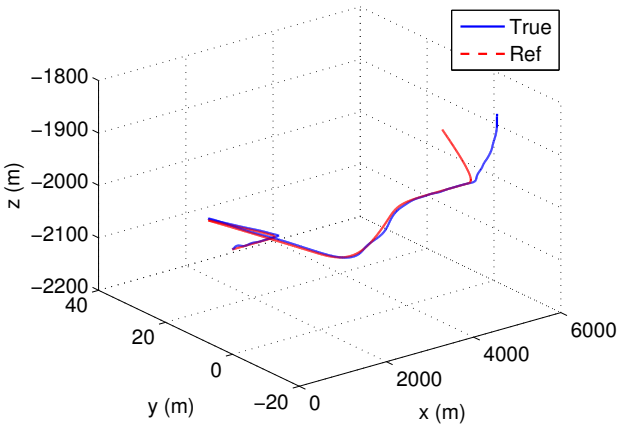

(a) Desired and true x, y and z

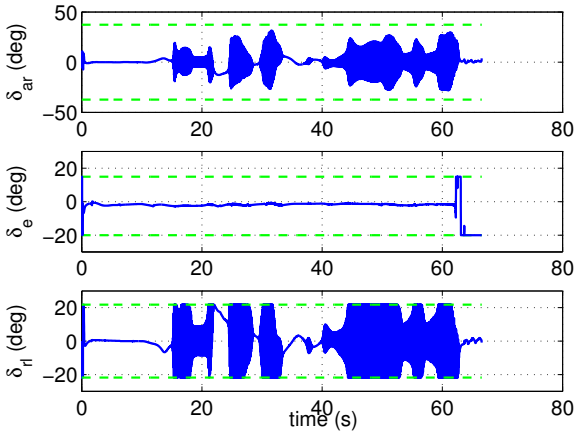

(b) δ_{ar}, δ_e and δ_{rl}, dashed lines represent the position limits.

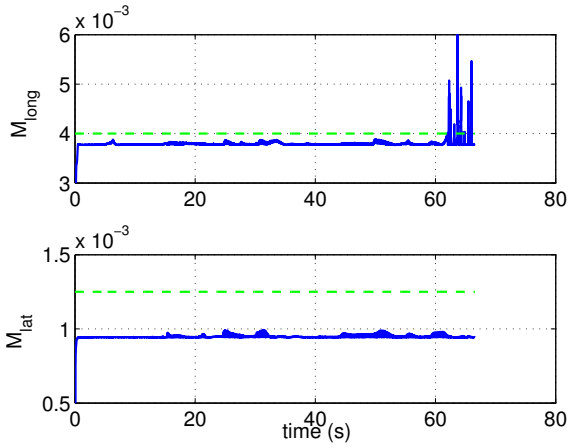

(c) M_{long} and M_{lat}, dashed lines represent the thresholds.

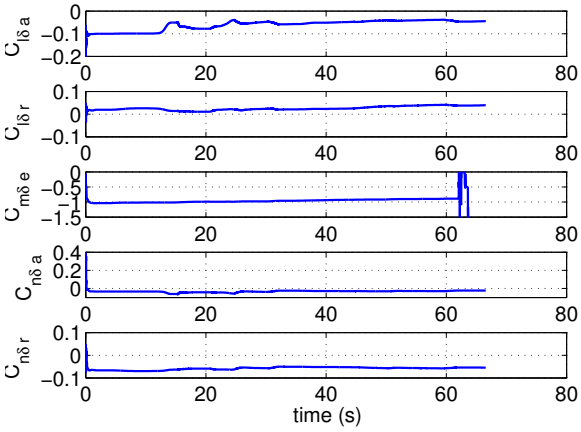

(d) Identified $C_{l\delta_a}$, $C_{l\delta_r}$, $C_{m\delta_e}$, $C_{n\delta_a}$ and $C_{n\delta_r}$

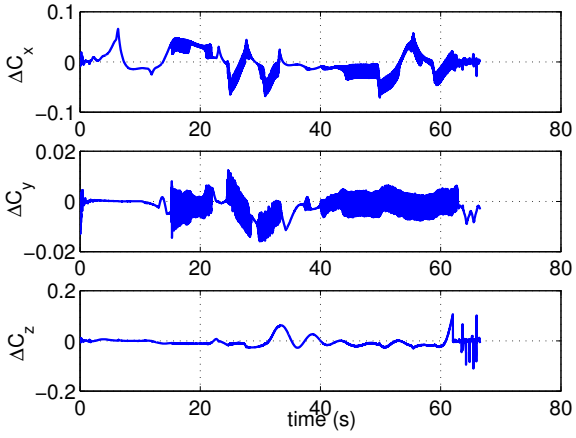

(e) ΔC_x, ΔC_y and ΔC_z

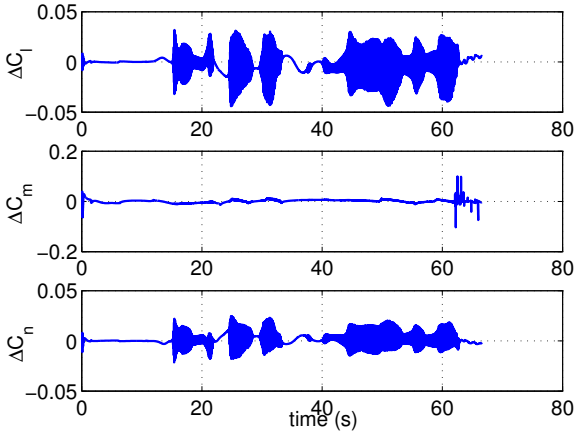

(f) ΔC_l, ΔC_m and ΔC_n

Figure 12: Results of aircraft trajectory control using the NDI-MI with thresholds (78) in the presence of model uncertainties.

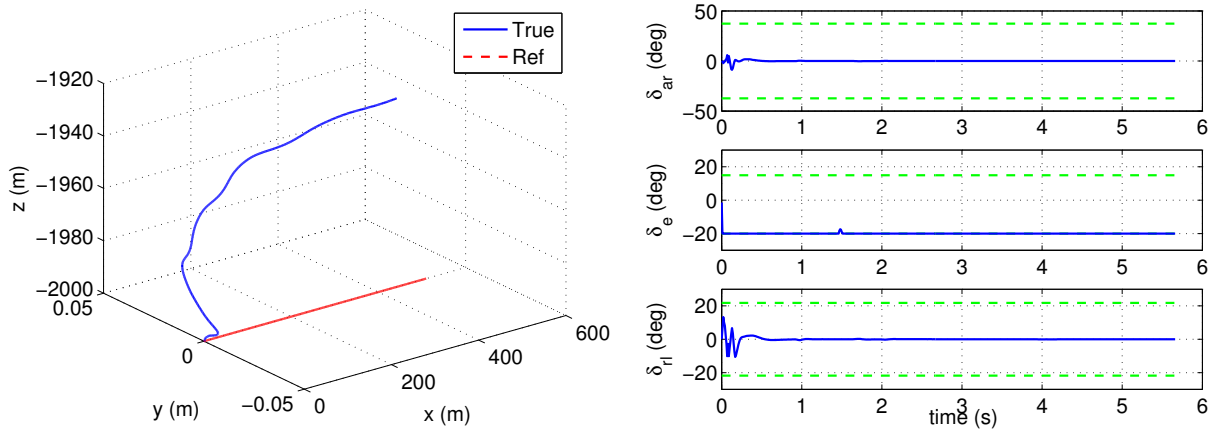

(a) Desired and true x, y and z

(b) δ_{ar}, δ_e and δ_{rl}, dashed lines represent the position limits.

Figure 13: Results of aircraft trajectory control using the NDI-MI in the presence of model uncertainties (parameters multiplied with 50%).

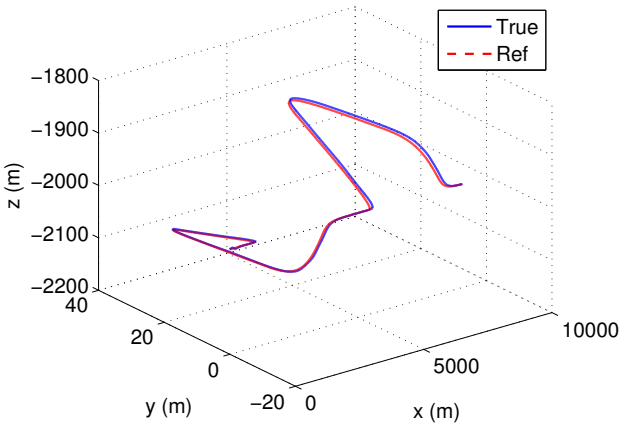

(a) Desired and true x, y and z

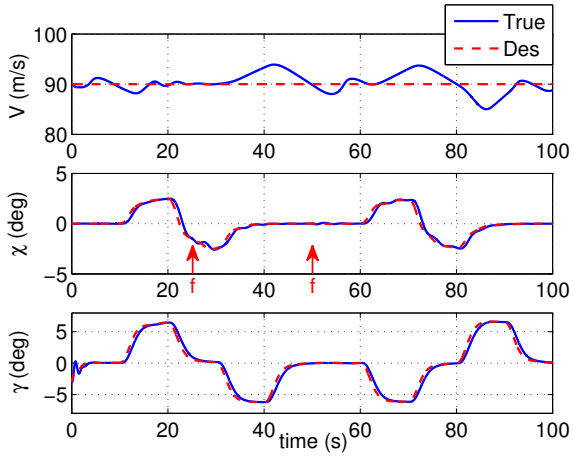

(b) Desired and true V, χ and γ

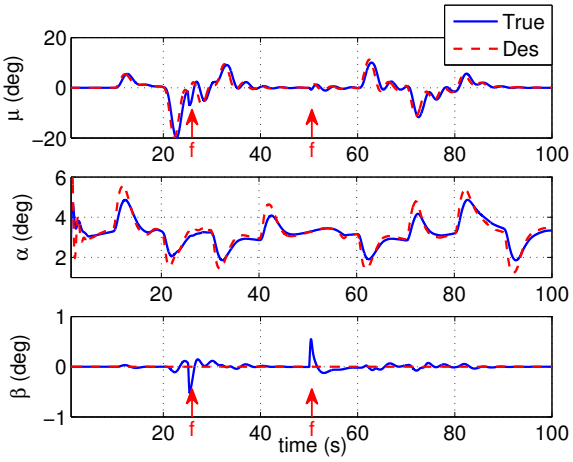

(c) Desired and true μ, α and β

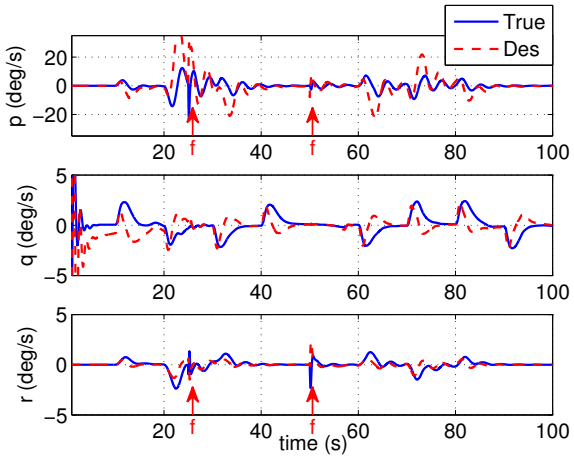

(d) Desired and true p, q and r

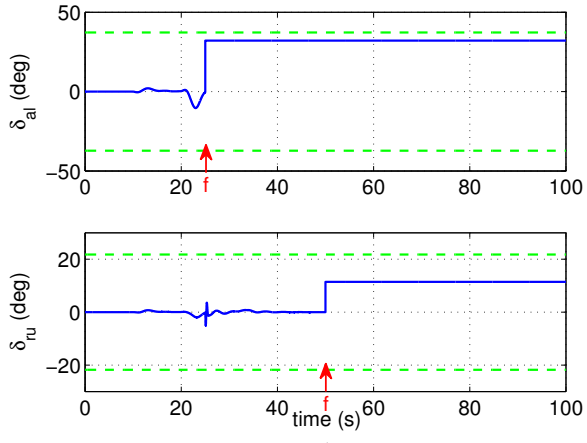

(e) δ_{al} and δ_{ru}, dashed lines represent the position limits.

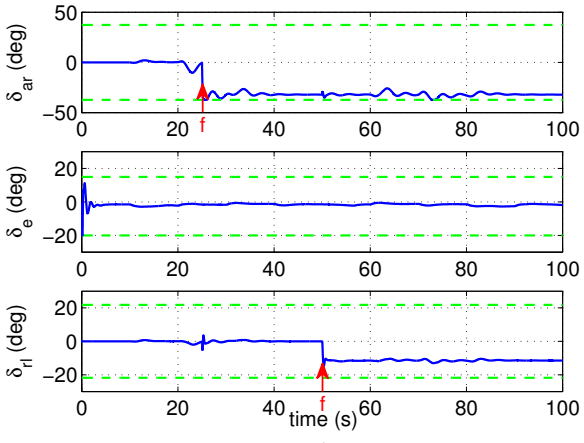

(f) δ_{ar}, δ_e and δ_{rl}, dashed lines represent the position limits.

Figure 14: Results of aircraft trajectory control using the INDI in the presence of model uncertainties and actuator faults.